

FIG. 1. Schematic diagrams of experiments in parkinsonian monkeys. Anatomical connections within cortico-BG circuits are shown. Open, filled and broken arrows represent glutamatergic, GABAergic and dopaminergic projections, respectively. The striatum (Str) and STN are two major input nuclei of the BG. Inputs from the cortex (Cx) and the thalamus (Th) enter the two nuclei and finally reach the GPI, an output nucleus of the BG. The GPe is positioned as an intermediate relay system, which is reciprocally interconnected with the STN. Dopaminergic projections from the substantia nigra pars compacta (SNc) are widely distributed in the BG. The following experiments were performed to examine the mechanisms regulating abnormal neuronal oscillations in the BG. (A) Single-unit recording of a GPI, a GPe or an STN neuron with intravenous injection of the dopamine precursor L-DOPA to restore dopamine levels (see Fig. 5 for GPI, Fig. 6 for GPe, and Fig. 7 for STN). (B) Recording from a GPI neuron with muscimol injection into the STN to block subthalamic inputs to the GPI (see Fig. 8). (C) Recording from a GPI (1) or a GPe (2) neuron with intrapallidal microinjection of the ionotropic glutamate receptor antagonists CPP and NBQX to block glutamatergic inputs to the GPI or GPe (see Fig. 9A–G for GPI and Fig. 9H–N for GPe). (D) Recording from a GPI (1) or a GPe (2) neuron with intrapallidal microinjection of the ionotropic GABA receptor antagonist gabazine to block GABAergic inputs to the GPI or GPe (see Fig. 10). Gabazine injection into the GPI blocked GABAergic inputs from the Str and GPe, and injection into the GPe blocked the inputs from the Str and GPe axon collaterals. (E) Recording from an STN neuron with intrasubthalamic microinjection of CPP and NBQX to block glutamatergic inputs to the STN (see Fig. 11). (F) Recording from an STN neuron with muscimol injection into the GPe to block GPe-derived GABAergic inputs (see Fig. 12).

goal of our study was to clarify the origin of GPI/GPe oscillations. Recordings of LFPs from PD patients show elevated levels of coherence between the STN and GPI (Brown *et al.*, 2001). The STN consists of glutamatergic projection neurons, and strongly influences GPI/GPe activity. To provide direct evidence that STN oscillations

may drive oscillations in the GPI/GPe, we performed single-unit GPI/GPe recordings while STN glutamatergic inputs were blocked (Fig. 1B and C). Finally, the origin of STN oscillations was also investigated. Glutamatergic inputs from the cerebral cortex and the thalamus may drive STN oscillations (Magill *et al.*, 2000, 2001;

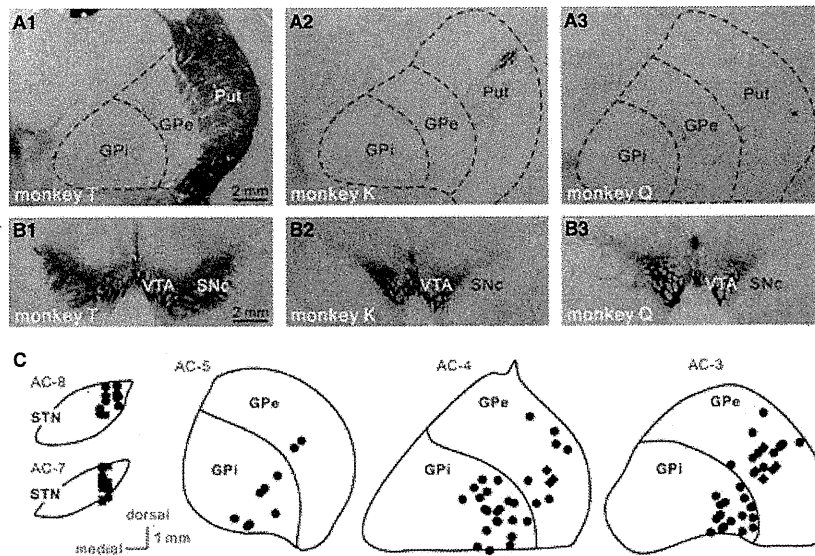


FIG. 2. TH immunoreactivity in the BG sampled from normal and MPTP-treated monkeys, and sites of unit recordings and drug injections in the STN and GPI/GPe. (A and B) Photomicrographs showing TH immunoreactivity in the putamen (Put; A1–A3) and the midbrain tegmentum (B1–B3). Sections in A1 and B1 are from a normal monkey (monkey T), and sections in A2, A3, B2 and B3 are from MPTP-treated monkeys (monkeys K and Q). As compared with the control (A1 and B1), marked reductions in TH immunoreactivity were observed in the Put (A2 and A3) and the ventral tier of the substantia nigra pars compacta (SNc) (B2 and B3) of the MPTP-treated monkeys. Note that numbers of TH-positive cells still remain in the dorsal tier of the SNc and the ventral tegmental area (VTA). The sections shown in A2 and A3 and the right side of the sections shown in B2 and B3 represent the sides ipsilateral to the carotid injections of MPTP and electrophysiological recordings. (C) Sites of unit recordings and drug injections in the STN and GPI/GPe are reconstructed from two MPTP-treated monkeys, and superimposed on representative coronal sections. Levels of the sections are indicated as distances (mm) from the caudal end of the anterior commissure (AC). Filled circles and squares represent the recording and injection sites, respectively. These sites are located within the motor territories of the STN and GPI/GPe (Nambu *et al.*, 2000; Tachibana *et al.*, 2008).

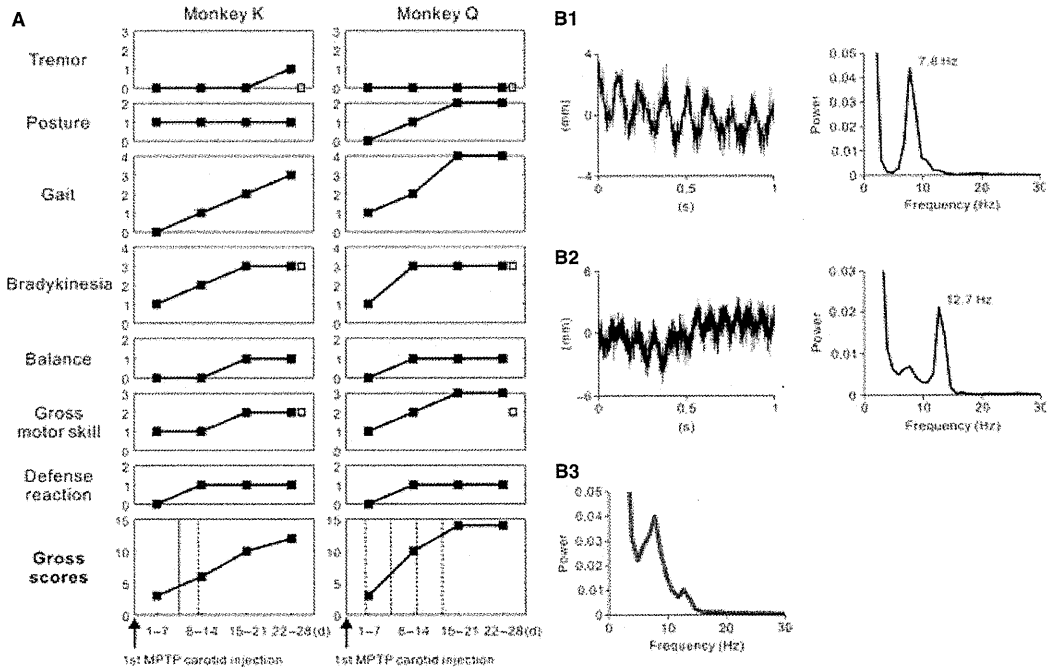


FIG. 3. Parkinsonian motor signs. (A) Parkinsonian rating scale. With the monkey parkinsonian rating scale of Smith *et al.* (1993), a variety of motor signs were evaluated (see also Supporting Information Data S1). Partial and gross motor scores are plotted along the time course (days) after the first carotid injection of MPTP. Filled and open squares represent the scores on the contralateral or ipsilateral side to the carotid injection, respectively. The solid vertical line for the gross scores represents the timing of the second MPTP carotid injection. The broken vertical lines represent the timings of additional intravenous MPTP injections. (B) Resting tremor in monkey K. Small forearm movements were detected with a laser displacement sensor (LK-500; sampling rate, 1 kHz; Keyence, Osaka, Japan). (B1 and B2) Two representative raw data of a 7.8-Hz dominant (B1) and a 12.7-Hz dominant (B2) tremor episode are shown in the left panels. The power spectra of each tremor episode are shown in the right panels. Power spectrum analyses were performed with 5-s raw data with a non-overlapping Hann window of 1024 bins, yielding a spectral resolution of 1 Hz. (B3) Averaged power spectrum from 41 tremor episodes, exhibiting two peaks at 7.8 and 12.7 Hz.

TABLE 1. Electrophysiological properties of GPe, GPi and STN neurons recorded before and after MPTP injections. (A) Monkey K. (B) Monkey Q

	GPe		GPi		STN	
	Normal (<i>n</i> = 51)	MPTP (<i>n</i> = 41)	Normal (<i>n</i> = 52)	MPTP (<i>n</i> = 32)	Normal (<i>n</i> = 47)	MPTP (<i>n</i> = 30)
(A)						
Firing rate (Hz)	64.7 ± 27.5	44.7 ± 23.1**	70.3 ± 26.0	73.0 ± 30.4	20.8 ± 11.4	30.7 ± 13.0***
Percentage of spikes in bursts (%)	14.0 ± 12.8	23.1 ± 17.2**	10.6 ± 11.3	22.7 ± 17.4***	24.4 ± 12.9	36.2 ± 12.0***
Mean 'surprise value'	4.30 ± 1.13	4.99 ± 2.11	4.32 ± 0.89	5.22 ± 2.33**	5.55 ± 1.50	5.71 ± 1.14
Number of 3–8-Hz oscillatory cells (%)	9/51 (17.6)	4/41 (9.8)	25/52 (48.1)	12/32 (37.5)	4/47 (8.5)	4/30 (6.7)
Mean 3–8-Hz power	1.09 ± 0.14	1.06 ± 0.12	1.26 ± 0.30	1.22 ± 0.43	1.04 ± 0.10	1.10 ± 0.13
Number of 8–15-Hz oscillatory cells (%)	0/51 (0.0)	4/41 (9.8)*	0/52 (0.0)	23/32 (71.9)***	4/47 (8.5)	10/30 (33.3)**
Mean frequency with maximum power at 8–15 Hz (Hz)	NA	12.6 ± 1.3 (<i>n</i> = 4)	NA	12.7 ± 1.3 (<i>n</i> = 23)	11.0 ± 2.2 (<i>n</i> = 4)	13.5 ± 0.6 (<i>n</i> = 10)
Mean 8–15-Hz power	0.82 ± 0.10	0.95 ± 0.13***	0.87 ± 0.10	1.31 ± 0.29***	0.97 ± 0.10	1.10 ± 0.13***
<hr/>						
	Normal (<i>n</i> = 54)	MPTP (<i>n</i> = 40)	Normal (<i>n</i> = 75)	MPTP (<i>n</i> = 68)	Normal (<i>n</i> = 44)	MPTP (<i>n</i> = 25)
(B)						
Firing rate (Hz)	65.6 ± 24.2	37.6 ± 21.6***	64.8 ± 22.9	58.4 ± 23.9	18.6 ± 7.6	23.9 ± 8.0*
Percentage of spikes in bursts (%)	14.7 ± 14.4	41.1 ± 24.1***	7.0 ± 7.0	20.2 ± 15.0***	32.6 ± 16.4	40.9 ± 14.9*
Mean 'surprise value'	4.53 ± 1.25	6.73 ± 3.15***	4.13 ± 0.97	4.98 ± 1.40**	5.36 ± 1.24	6.14 ± 1.72*
Number of 3–8-Hz oscillatory cells (%)	17/54 (31.5)	11/40 (27.5)	28/75 (37.3)	28/68 (41.2)	1/44 (2.2)	4/25 (16.0)*
Mean 3–8-Hz power	1.13 ± 0.24	1.18 ± 0.17	1.15 ± 0.25	1.18 ± 0.28	1.00 ± 0.19	1.13 ± 0.20**
Number of 8–15-Hz oscillatory cells (%)	0/54 (0.0)	4/40 (10.0)*	0/75 (0.0)	23/68 (33.8)***	2/44 (4.5)	6/25 (24.0)*
Mean frequency with maximum power at 8–15 Hz (Hz)	NA	10.7 ± 0.8 (<i>n</i> = 4)	NA	11.4 ± 1.0 (<i>n</i> = 23)	11.7 ± 3.5 (<i>n</i> = 2)	10.7 ± 1.9 (<i>n</i> = 6)
Mean 8–15-Hz power	0.79 ± 0.13	0.87 ± 0.13*	0.76 ± 0.11	1.05 ± 0.36***	0.94 ± 0.17	1.02 ± 0.15*

Firing properties of GPe, GPi and STN neurons are represented as mean ± SD. Mann–Whitney *U*-tests were performed between normal and parkinsonian states. The proportions of oscillatory cells were compared by use of Fisher's exact tests. NA, data not available. Significance levels are as follows: **P* < 0.05, ***P* < 0.01, ****P* < 0.001.

Williams *et al.*, 2002; Sharott *et al.*, 2005; Mallet *et al.*, 2008b). It has also been demonstrated by Baufreton *et al.* (2005a) that excitation together with feedback GABAergic inhibition from the GPe is sufficient to generate highly synchronous activity (15–30 Hz) of STN neurons *in vitro*. However, it is unknown how the glutamatergic and pallidal GABAergic inputs contribute to STN oscillations. To address this issue, we examined STN activity during blockade of the two synaptic inputs (Fig. 1E and F). We found that, in the dopamine-depleted state, the oscillatory activity of STN neurons is generated by both the glutamatergic and the GPe-derived GABAergic inputs, and finally transmitted to the GPi.

Materials and methods

Surgical procedures

Two male monkeys (*Macaca cyclopis*, monkey K, and *Macaca mulatta*, monkey Q) weighing 3.5–5.0 kg were used as subjects in this study. The experimental protocols were approved by the Institutional Animal Care and Use Committee of National Institutes of Natural Sciences, and all experiments were conducted according to the guidelines of the National Institutes of Health *Guide for the Care and Use of Laboratory Animals*.

Prior to the experiments, each monkey was trained to sit quietly in a monkey chair. Under general anesthesia with intramuscular ketamine hydrochloride (10 mg/kg body weight) and intravenous sodium pentobarbital (25 mg/kg), the monkeys underwent a surgical procedure for head fixation and extracellular recordings of GPi/GPe and STN neurons, as reported previously (Nambu *et al.*, 2000; Tachibana *et al.*, 2008). Magnetic resonance imaging (3T Allegra; Siemens, Erlangen, Germany) scans were performed to estimate stereotaxic coordinates of the brain structures. Recordings of neuronal activity in the GPi/GPe and STN under normal conditions were initiated 2 weeks after the initial surgery.

Electrophysiological recording

During the recording sessions, each monkey was in an awake state and seated in the monkey chair with his head restrained. Single-unit recordings of GPi/GPe and STN neurons were performed with a glass-coated Elgiloy microelectrode (0.8–1.2 M Ω at 1 kHz for GPi/GPe; 1.5–2.0 M Ω for STN). The electrode was inserted obliquely (45° from vertical in the frontal plane) into the GPi/GPe or vertically into the STN with a hydraulic microdrive. The unitary activity recorded from the microelectrode was amplified ($\times 8000$), filtered (100 Hz to 2 kHz), converted into digital data with a window discriminator, and sampled at 2 kHz with a computer. In this study, we examined neuronal populations sampled from the motor territories (forelimb and orofacial regions) of the GPi/GPe and STN (Nambu *et al.*, 2000; Tachibana *et al.*, 2008); the recording sites were located in the lateral parts of individual structures at their middle to caudal levels (Fig. 2C). The subdivisions of the pallidum (i.e. GPe and GPi) were determined by the depth of recording electrodes, firing patterns and decreased electrical signals in the lamina between the GPe and GPi (Nambu *et al.*, 2000). The monkey's arousal level was visually monitored and maintained during recording sessions. Only stable and well-isolated neurons were included in the present data.

MPTP injections

After the recordings of GPi/GPe and STN neurons in the normal state, systemic administration of MPTP (Sigma, St Louis, MO, USA) was

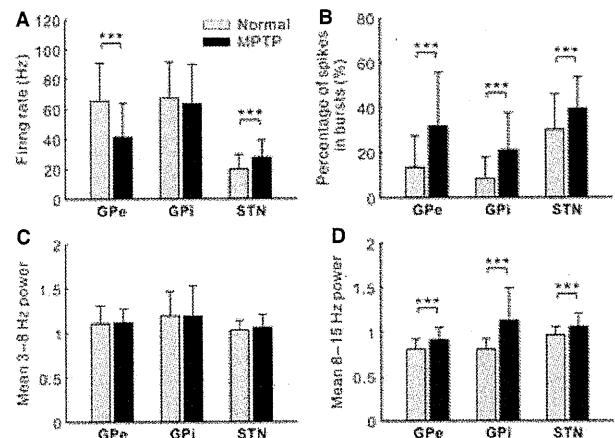


FIG. 4. Comparison of electrophysiological properties of BG neurons in normal and parkinsonian monkeys. (A) Spontaneous firing rates. Gray and black columns show the average firing rates in normal and MPTP-treated monkeys, respectively. Data are given as mean \pm SD. The same conventions are used in B–D. The GPe firing rate was significantly decreased after MPTP treatment, whereas the STN firing rate was significantly increased. (B) Percentage of spikes in bursts. The bursts were detected with the ‘Poisson surprise’ algorithm. The burst strength was increased in all three structures. (C) Averaged power of 3–8-Hz oscillatory activity. Oscillatory activity was calculated on the basis of the algorithm of Rivlin-Etzion *et al.* (2006b). There were no changes in 3–8-Hz oscillatory activity. (D) Averaged power of 8–15-Hz oscillatory activity. Significant increases in 8–15-Hz oscillatory power were detected in all three structures. The pooled data from two monkeys were the same as those for the neuronal populations in Table 1. *** $P < 0.001$.

performed under the same general anesthesia as described above (Kaneda *et al.*, 2005). The MPTP injection (1.2 mg/kg) unilateral to the recording side was made through the common carotid artery with the external carotid artery clamped (Fig. 2A and B). With the monkey parkinsonian rating scale (Smith *et al.*, 1993; see also Supporting Information Data S1), motor signs were quantitatively evaluated (the maximum parkinsonian score was 20; that is, more serious parkinsonian stages were indicated by higher scores; Fig. 3A). To make moderate to severe parkinsonian models, monkeys received an additional carotid artery injection (1.0 mg/kg, 1 week after the first injection) and/or intravenous injections through the great saphenous vein (0.3 mg/kg every 4 days, 3 days after the last carotid injection). Monkey K received carotid injections twice (1.2 and 1.0 mg/kg) and intravenous injection once, and monkey Q received carotid injection once and intravenous injection four times. The total doses of MPTP were 2.5 mg/kg for monkey K and 2.4 mg/kg for monkey Q. Unit recordings of BG neurons in the parkinsonian state was started after the parkinsonian scores became stable, that is, 2 weeks (monkey K) and 3 weeks (monkey Q) after the final MPTP injection.

L-DOPA treatments

We investigated the effects of systemic dopamine administration on the neuronal activity of GPi/GPe and STN neurons in the parkinsonian state. After the control recordings of GPi/GPe and STN neurons, 3.5 mg/kg (monkey K) or 2.5 mg/kg (monkey Q) L-DOPA (DOPASTON, a dopamine precursor; Sankyo, Tokyo, Japan) was manually injected into the great saphenous vein at a low rate, and this was followed by the infusion of electrolyte fluid. To verify the contingency between the L-DOPA-induced behavioral effects and the activity changes in BG neurons, we avoided using Carbidopa, which could prevent the conversion of L-DOPA to dopamine peripherally and delay

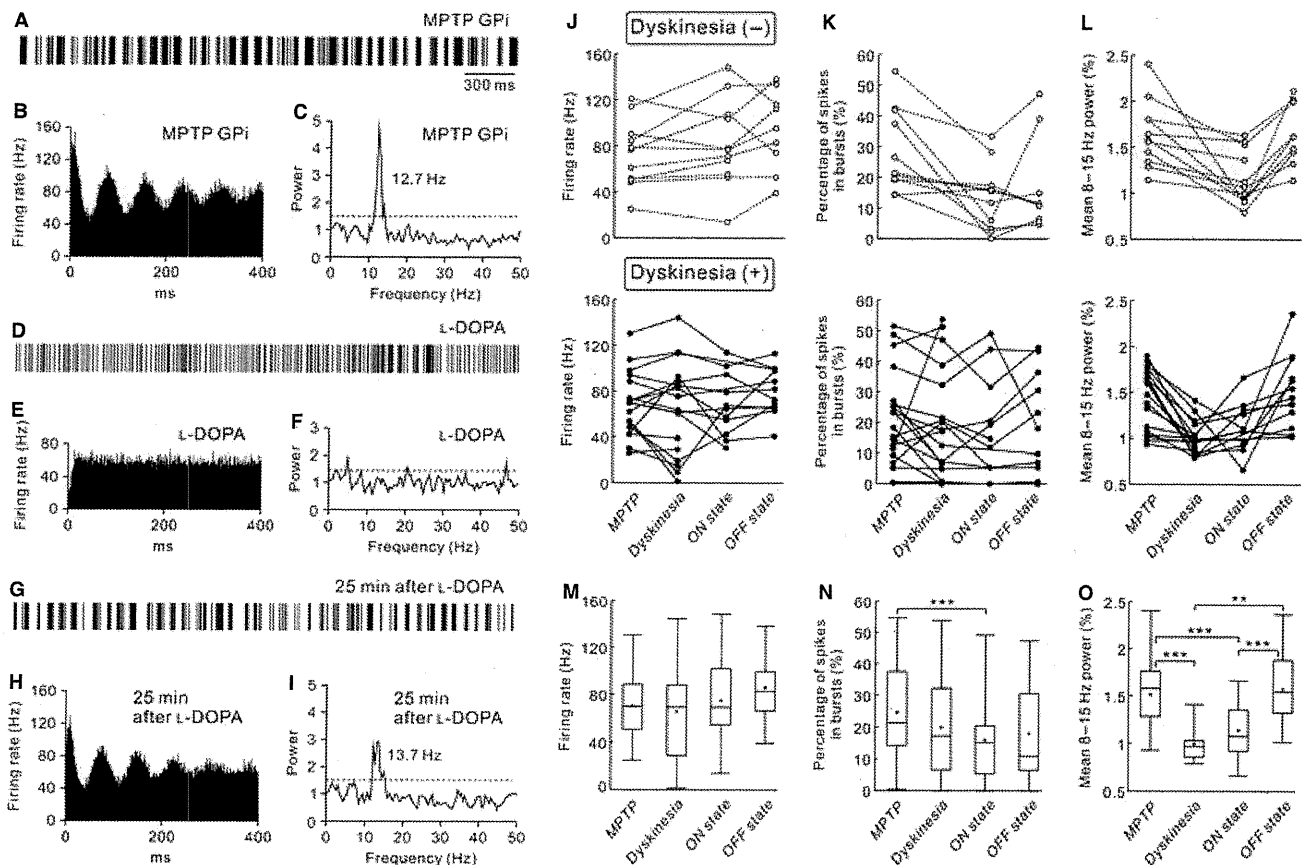


FIG. 5. L-DOPA effects on dopamine-depleted GPI neurons. (A, D and G) Representative 3-s digitized spikes from a 50-s spike train before and after intravenous L-DOPA injection. (B, E and H) Autocorrelograms calculated from the same spike train (bin width, 0.5 ms). (C, F and I) Power spectra of the same spike trains, compensated by the algorithm of Rivlin-Etzion *et al.* (2006b). Gray dashed lines represent a confidence level of $P = 0.01$. Peak frequency in the range of 8–15 Hz is also shown. A GPI neuron showed 8–15-Hz oscillations in the parkinsonian state (A–C). An intravenous L-DOPA injection reduced the 8–15-Hz oscillatory activity in the GPI (D–F), with an improvement in parkinsonian motor signs (ON state). Twenty-five minutes after the L-DOPA injection, the oscillatory activity resumed (G–I). At this time, recuperation from the parkinsonism was not observed (OFF state). (J–L) Changes in the spontaneous firing rate (J), the burst strength (K) and the mean 8–15-Hz power spectrum of spike trains (L) after the L-DOPA injections. The upper rows show the neurons recorded without dyskinesia. The lower rows show the neurons recorded with the development of dyskinesia. Data are plotted along the behavioral changes, and the data points from the same neuron are connected with lines. Owing to the excessive body movement of the monkeys, some GPI neurons were lost during neuronal recording. (M–O) Summaries of the L-DOPA effects on the firing rate (M), the burst strength (N) and the mean 8–15-Hz power (O) in 29 GPI neurons examined. In box plots, means are indicated as black dots. In this and subsequent figures, the repeated Wilcoxon signed-rank tests were performed to calculate statistically significant differences among pre-injection (labeled as MPTP) and post-injection (dyskinesia, ON state and OFF state) conditions. In the GPI neurons tested, the overall firing rate did not change throughout the injections. In contrast, the power of 8–15-Hz oscillations was significantly decreased from pre-injection states to dyskinetic states and to ON states. A significant decrease in the burst strength was also detected between pre-injection states and ON states. ** $P < 0.01$, *** $P < 0.001$.

the termination of the L-DOPA effects. An optimal dose of L-DOPA was determined so that the injection would reduce the gross parkinsonian scores by 5 or more. The L-DOPA effects on neuronal activity in the GPI/GPe and STN appeared within approximately 5 min. During this period, the L-DOPA greatly improved the motor symptoms of both monkeys, and eventually induced dyskinetic movements (dyskinetic state). The dyskinesia typically appeared as oral dyskinesia and/or forelimb dyskinesia, and sometimes spread to entire body parts. The excessive dyskinetic state usually ceased in 5–10 min and shifted to the ON state without dyskinesia, termed the ‘ON state’. Approximately 30 min after the injection, the animals exhibited the original parkinsonism, termed the ‘OFF state’. In some cases, the L-DOPA effects appeared without development of the dyskinetic state. The L-DOPA experiments were limited to two injections per recording day, and the interval between the injections was >2 h throughout the experiments. It should be noted that the electrophysiological data for the dopamine-depleted state in Table 1 were collected before the following receptor-

related drug injection experiments (monkey K, including the neurons sampled at least 48 h after the last L-DOPA injection; monkey Q, including the neurons recorded only in the L-DOPA-naive state).

Unit recordings with local drug injection

We developed a microinjection method to examine the impacts of direct synaptic inputs (i.e. glutamatergic and GABAergic inputs) on the oscillatory activity of individual BG neurons. Unit recordings of GPI/GPe or STN neurons with local drug injection were performed with an electrode assembly consisting of a glass-coated Elgiloy microelectrode for unit recording and a silica tube for drug delivery, as described previously (Tachibana *et al.*, 2008). Through the silica tube, one of the following drugs was injected (0.03–0.05 $\mu\text{L}/\text{min}$; total, 0.1–0.2 μL): (i) a mixture of an *N*-methyl-D-aspartate receptor antagonist, 3-(2-carboxypiperazin-4-yl)-propyl-1-phosphonic acid (CPP) (1 mM; Sigma), and an AMPA/kainate

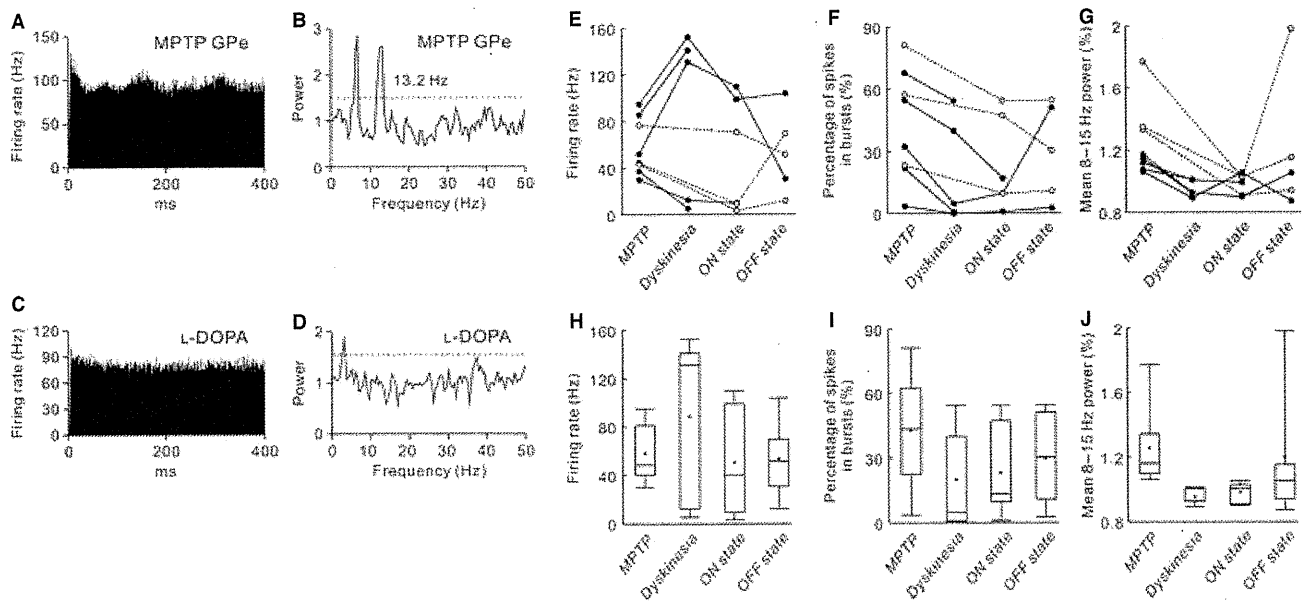


FIG. 6. L-DOPA effects on dopamine-depleted GPe neurons. (A and B) A GPe neuron showed 3–8-Hz and 8–15-Hz oscillations in the parkinsonian state. The conventions in this and the following figures are the same as in Fig. 5. (C and D) An intravenous L-DOPA injection suppressed both types of oscillation in the GPe neuron. (E–G) L-DOPA-induced changes in the spontaneous firing rate (E), the burst strength (F) and the mean 8–15-Hz power (G) of eight GPe neurons tested. Data from the neurons recorded without dyskinesia (open circles and broken lines) are superimposed on those from the neurons recorded with dyskinesia (filled circles and solid lines). (H–J) Summaries of the L-DOPA effects on the firing rate (H), the burst strength (I) and the mean 8–15-Hz power (J) in GPe neurons.

receptor antagonist, 1,2,3,4-tetrahydro-6-nitro-2,3-dioxo-benzo[*f*]quinoxaline-7-sulfonamide (NBQX) (1 mM; Sigma); and (ii) a GABA_A receptor antagonist, gabazine (1 mM; Sigma). Injection sites were located at least 1 mm apart because the effective radius of the drugs was estimated to be approximately 1 mm (Tachibana *et al.*, 2008). This method limited unit recordings to a maximum of two GPi/GPe neurons or a single STN neuron per recording day.

Methods for inactivation of the STN or GPe were similar to the methods described elsewhere (Nambu *et al.*, 2000; Tachibana *et al.*, 2008). A Teflon-coated tungsten wire that was attached to the 31-gauge needle of a 10- μ L Hamilton microsyringe, or the above electrode assembly, was inserted vertically into the STN or obliquely into the GPe with a hydraulic microdrive. A GABA_A receptor agonist, muscimol (4.4 mM; 0.5–1.0 μ L in the STN, 1–2 μ L in the GPe; Sigma), was injected. Because the effect of muscimol on the target structure lasted for several hours, the inactivation of the STN or GPe was limited to a single injection per recording day.

Data analysis

Off-line data analysis was performed with MATLAB software (MathWorks, Natick, MA, USA). Spontaneous firing rates and patterns of the recorded neurons were analyzed by calculating the autocorrelograms (bin width, 0.5 ms) from 50 s of digitized recordings.

Bursts of GPi/GPe and STN neurons were detected on the basis of the 'Poisson surprise' algorithm, with a 'surprise value' of at least three and a number of spikes of at least three in a burst (Wichmann & Soares, 2006; see also Supporting Information Fig. S1). Briefly, the algorithm can calculate a probability that successive spikes occur in a given time window of a spike train, which is assumed to be Poisson-distributed with the same firing rate. If the successive spikes occur with a significantly low probability ('surprise'), the spikes are considered as a burst. The strength of bursts was estimated by the

percentage of spikes in bursts (as compared with all spikes in the recording data), which has frequently been used in other studies (Levy *et al.*, 2001a; Wichmann & Soares, 2006). We also calculated the mean 'surprise value' of overall bursts detected by the algorithm. Oscillatory activity of GPi/GPe and STN neurons was estimated by spectral analysis of spike trains with a shuffling technique (Rivlin-Etzion *et al.*, 2006b). The method calculated the power spectral density (PSD) of spike trains based on Welch's method (Halliday *et al.*, 1995). The PSD calculation was performed with a non-overlapping Hann window with a length of 4096 bins. Because the sampling frequency of spike trains was 2 kHz, the frequency resolution was approximately 0.5 Hz. In the present study, the compensated PSD was obtained from the PSD of original spike trains divided by the mean PSD of locally ($T = 175$ – 225 ms) shuffled ($n = 50$) spike trains. The local shuffling method minimized the spectral distortion at lower frequencies caused by the refractory periods of neurons, and the effect of the neuronal firing rate on the PSD, thus enabling easy detection of periodic oscillatory phenomena in the recorded neurons. A confidence level ($P < 0.01$) of the compensated PSD was determined on the basis of the mean \pm standard deviation (SD) of the PSD values in the range of 270–300 Hz, at which the PSD values were stable. Oscillatory cells were defined by determining whether their two consecutive PSD values within individual ranges of 3–8 and 8–15 Hz crossed the confidence level (Soares *et al.*, 2004). The power (strength) of 3–8- and 8–15-Hz oscillations was estimated by averaging the PSD values within the individual frequency bands, and termed 'mean 3–8-Hz power' and 'mean 8–15-Hz power', respectively. We also estimated the oscillatory activity in the range of 20–30 Hz in the same manner.

Histology

At the end of the final recordings, reference lesions were placed at several sites by passing a cathodal DC current of 20 μ A through the

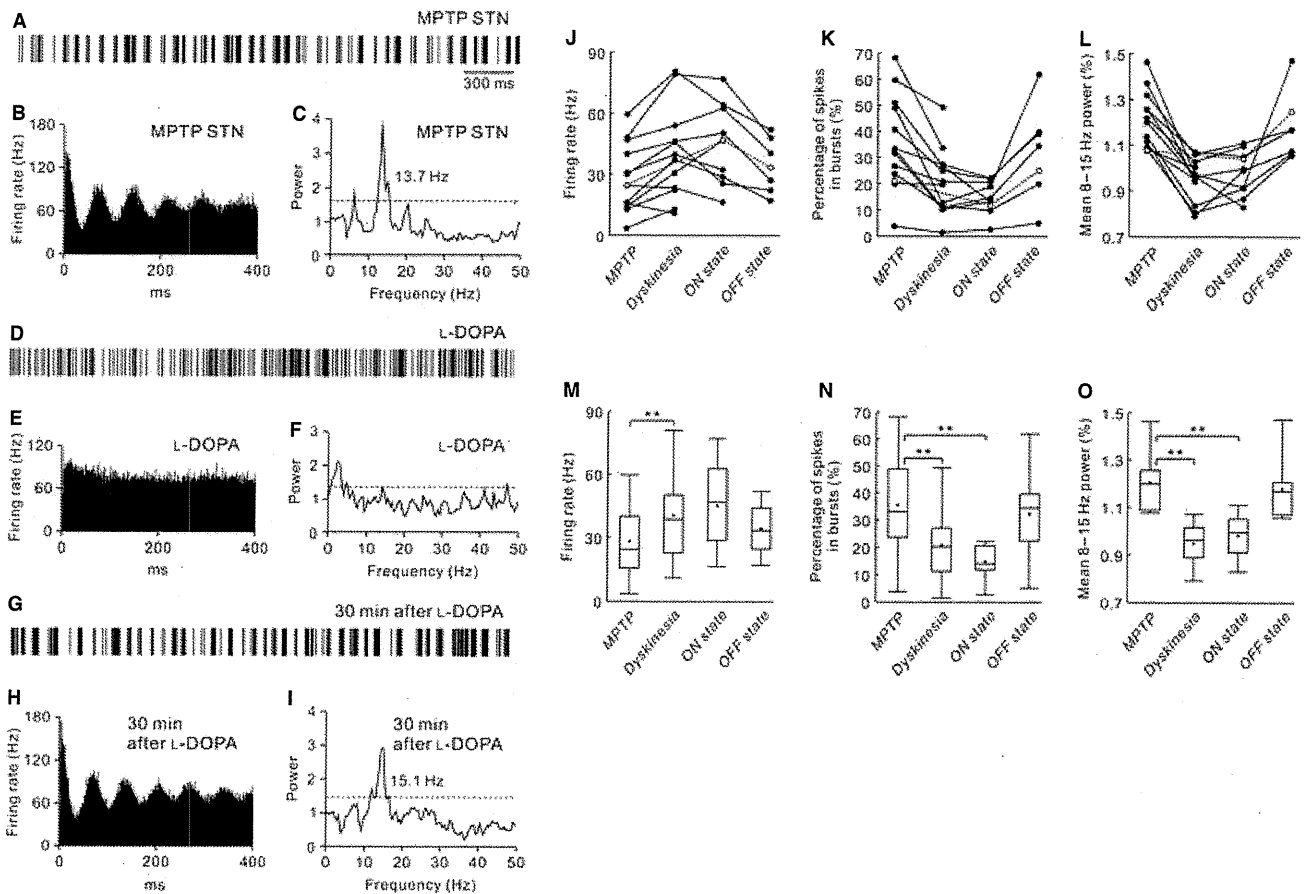


FIG. 7. L-DOPA effects on dopamine-depleted STN neurons. (A–C) An STN neuron showed oscillations in the parkinsonian state. (D–F) An intravenous L-DOPA injection increased the firing rate and suppressed the 8–15-Hz oscillatory activity of the STN neuron during the ON state. In this example, 3–8-Hz oscillations were also attenuated. (G–I) Thirty minutes after the L-DOPA injection, the oscillatory activity appeared again. (J–L) L-DOPA-induced changes in the spontaneous firing rate (J), the burst strength (K) and the mean 8–15-Hz power (L) of 13 STN neurons tested. Data from the neuron recorded without dyskinesia (open circles and broken lines) are superimposed on those from the neurons recorded with dyskinesia (filled circles and solid lines). (M–O) Summaries of the L-DOPA effects on the firing rate (M), the burst strength (N) and the mean 8–15-Hz power (O) in the STN neurons. The average firing rate was increased from pre-injection states to dyskinetic states. On the other hand, there were significant decreases in the burst strength and the mean power of 8–15-Hz oscillations from pre-injection states to dyskinetic states and to ON states. $**P < 0.01$.

electrode for 30 s. The monkeys were deeply anesthetized with intravenous sodium pentobarbital (50 mg/kg) and perfused transcardially with the same methods as reported previously (Kaneda *et al.*, 2005). Serial 60- μ m sections were processed for Nissl staining or tyrosine hydroxylase (TH) immunostaining by the same methods as described elsewhere (Kaneda *et al.*, 2005; Tachibana *et al.*, 2008). The recording and drug injection sites were confirmed according to the lesions made by the cathodal DC current and the traces of electrode tracks.

Statistical analysis

All of the data are represented as mean \pm SD. Statistical tests were performed with SPSS (IBM, Armonk, NY, USA). Because we made an effort to minimize the damage to brain tissues caused by drug injections, the sample size was not large throughout the experiments. Therefore, we performed a non-parametric Wilcoxon signed-rank test or Mann–Whitney *U*-test for all neuronal data sets. The proportions of oscillatory cells in normal and parkinsonian states were compared by the use of Fisher's exact test. Significance levels were generally set as $P = 0.05$. In the studies with L-DOPA injections, however, we set the

significant levels at $P = 0.01$, because the Wilcoxon signed-rank tests were repeatedly performed.

Results

Behavioral and neuronal changes after MPTP injections

We produced the primate model of PD via a unilateral MPTP injection into the internal carotid artery and additional intravenous injections of MPTP. TH immunohistochemistry confirmed the loss of dopaminergic terminals in the putamen and dopaminergic neurons in the substantia nigra of the two MPTP-treated monkeys that served as subjects in this study (Fig. 2A and B). The reduction in TH immunoreactivity was more prominent in the ventral and lateral portions than in the dorsal and medial portions of the substantia nigra of MPTP-treated monkeys; selective loss of dopaminergic neurons by MPTP induction is commonly observed in human PD patients (Yamada *et al.*, 1990; Kaneda *et al.*, 2003). Both monkeys showed obvious parkinsonian signs, such as akinesia/bradykinesia, rigidity, and flexed posture, more severely on the side of the body contralateral to the carotid artery MPTP injection (Fig. 3A). Monkey

parkinsonian scores (Smith *et al.*, 1993; see also Supporting Information Data S1) of the contralateral side to the carotid injections were 11–12 in monkey K (contralateral side: tremor, 0–1/3; posture, 1/2; gait, 3/4; bradykinesia, 3/4; balance, 1/2; gross motor skill, 2/3; defense reaction, 1/2) (ipsilateral side: tremor, 0/3; bradykinesia, 3/4; gross motor skill, 2/3) and 13–14 in monkey Q (contralateral side: tremor, 0/3; posture, 2/2; gait, 3–4/4; bradykinesia, 3/4; balance, 1/2; gross motor skill, 3/3; defense reaction, 1/2) (ipsilateral side: tremor, 0/3; bradykinesia, 3/4; gross motor skill, 2/3). Monkey K occasionally showed weak limb tremor, with peak frequencies of 7.8 and 12.7 Hz (Fig. 3B) (see also Heimer *et al.*, 2006), whereas monkey Q showed no visible tremor. The parkinsonian scores were stable throughout the recording sessions.

Figure 4 and Table 1 show the electrophysiological properties of BG neurons in the normal and parkinsonian states. As compared with the normal state, the average firing rates of GPe and STN neurons in the parkinsonian state were significantly decreased and increased, respectively. However, no changes were detected in the firing rate of GPI neurons. Burst strength was increased from the normal to the parkinsonian state in the GPe, GPI, and STN. Both parkinsonian monkeys showed increases in the number of neurons that oscillated in the 8–15-Hz range in all three of the structures, whereas there were no consistent changes in the number of 3–8-Hz oscillatory cells. The mean power of the 8–15-Hz oscillations increased in all of the structures. Indeed, neurons in the GPI and STN of the two parkinsonian monkeys displayed remarkable tendencies to produce oscillatory bursts, as shown by rhythmic spike trains, and multiple peaks in the autocorrelograms, and power spectrum (e.g. Figs 5A–C and 7A–C). Although the power of 8–15-Hz oscillations in the GPe tended to be weaker than those in the GPI and STN, the oscillatory bursts were also observed in GPe neurons (Fig. 6). The peak frequency with a maximum power of the oscillatory bursts was approximately 13 Hz in all three structures in both monkeys. We also analyzed the power of 20–30-Hz oscillatory activity in the BG, but we did not find a significant increase from normal to parkinsonian conditions (monkey K, GPe, 0.87 ± 0.08 to 0.87 ± 0.15 ; monkey K, GPI, 0.86 ± 0.12 to 0.77 ± 0.14 ; monkey K, STN, 0.95 ± 0.06 to 0.84 ± 0.13 ; monkey Q, GPe, 0.83 ± 0.18 to 0.79 ± 0.15 ; monkey Q, GPI, 0.90 ± 0.12 to 0.81 ± 0.16 ; monkey Q, STN, 0.96 ± 0.08 to 0.84 ± 0.13 ; mean \pm SD). Thus, for the following drug injection studies, we pooled the neuronal data from two monkeys and focused on the 8–15-Hz oscillations.

Dopamine dependence of 8–15-Hz oscillations in the BG

We examined the effects of systemic dopamine administration on the neuronal activity of GPI/GPe and STN neurons under parkinsonian conditions (Fig. 1A). Across the L-DOPA injections tested, the behavioral effects appeared within 5 min, and parkinsonian motor scores (such as tremor, bradykinesia, and gross motor skill) were improved by 3–5 (ON state). In more than half of the cases, the animals developed dyskinetic movements in the orofacial and/or forelimb areas prior to the ON state (see Materials and methods). The excessive dyskinetic states usually ceased in 5–10 min. Approximately 30 min after each injection, the animals showed the original parkinsonism (OFF state). In a representative GPI neuron, an intravenous L-DOPA injection decreased the 8–15-Hz oscillations in the ON state (Fig. 5A–F), and the abnormal oscillations appeared again in the OFF state (Fig. 5G–I). In 29 GPI neurons examined, the overall firing rate was not changed throughout the injections (Fig. 5M; Wilcoxon signed-rank test). In contrast, the mean power

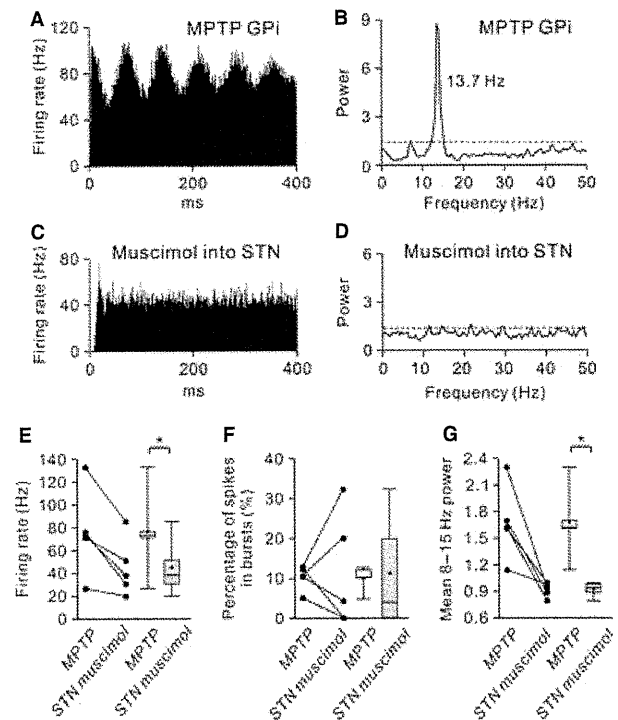


FIG. 8. Effects of STN inactivation on dopamine-depleted GPI neurons. (A and B) A GPI neuron showed abnormal oscillations in the parkinsonian state. (C and D) Muscimol inactivation of the STN decreased the firing rate, and suppressed 8–15-Hz oscillatory activity in the GPI. (E–G) Summaries of the effects of muscimol inactivation of the STN on the spontaneous firing rate (E), the burst strength (F) and the mean 8–15-Hz power spectrum of spike trains (G) in five GPI neurons examined. The STN inactivation significantly decreased the firing rate and the 8–15-Hz power of oscillations in the GPI. * $P < 0.05$.

of 8–15-Hz oscillations was significantly decreased from pre-injection states to dyskinetic states (Fig. 5O; $P < 0.001$, Wilcoxon signed-rank test) and to ON states ($P < 0.001$). Significant decreases in the burst strength were also detected between pre-injection states and ON states (Fig. 5N; $P < 0.001$, Wilcoxon signed-rank test). Although there was a tendency for the power of 8–15-Hz oscillations in dyskinetic states to be lower than that in ON states, we did not detect significant differences in the three parameters (i.e. firing rate, burst strength, and 8–15-Hz oscillatory power) between dyskinetic states and ON states. Similarly, the decreases in abnormal oscillatory bursts of GPe neurons were observed after L-DOPA injections, even though the average firing rate did not change across the recorded population (Fig. 6).

L-DOPA administration also suppressed 8–15-Hz oscillations in the STN (Fig. 7A–F). The abnormal oscillations were concomitant with the re-emergence of parkinsonian motor signs (Fig. 7G–I). In contrast to what was found for GPI/GPe neurons, the average firing rate of 13 STN neurons tested was increased from pre-injection states to dyskinetic states (Fig. 7M; $P = 0.005$). On the other hand, significant decreases in the burst strength (Fig. 7N) and the mean power of 8–15-Hz oscillations (Fig. 7O) were observed from pre-injection states to dyskinetic states ($P = 0.002$ for burst strength; $P = 0.002$ for 8–15-Hz oscillatory power) and to ON states ($P = 0.002$ for burst strength; $P = 0.008$ for 8–15-Hz oscillatory power). Thus far, we have demonstrated that abnormal burst firing and 8–15-Hz oscillatory activity in the GPI/GPe and STN are related to dopamine deficiency.

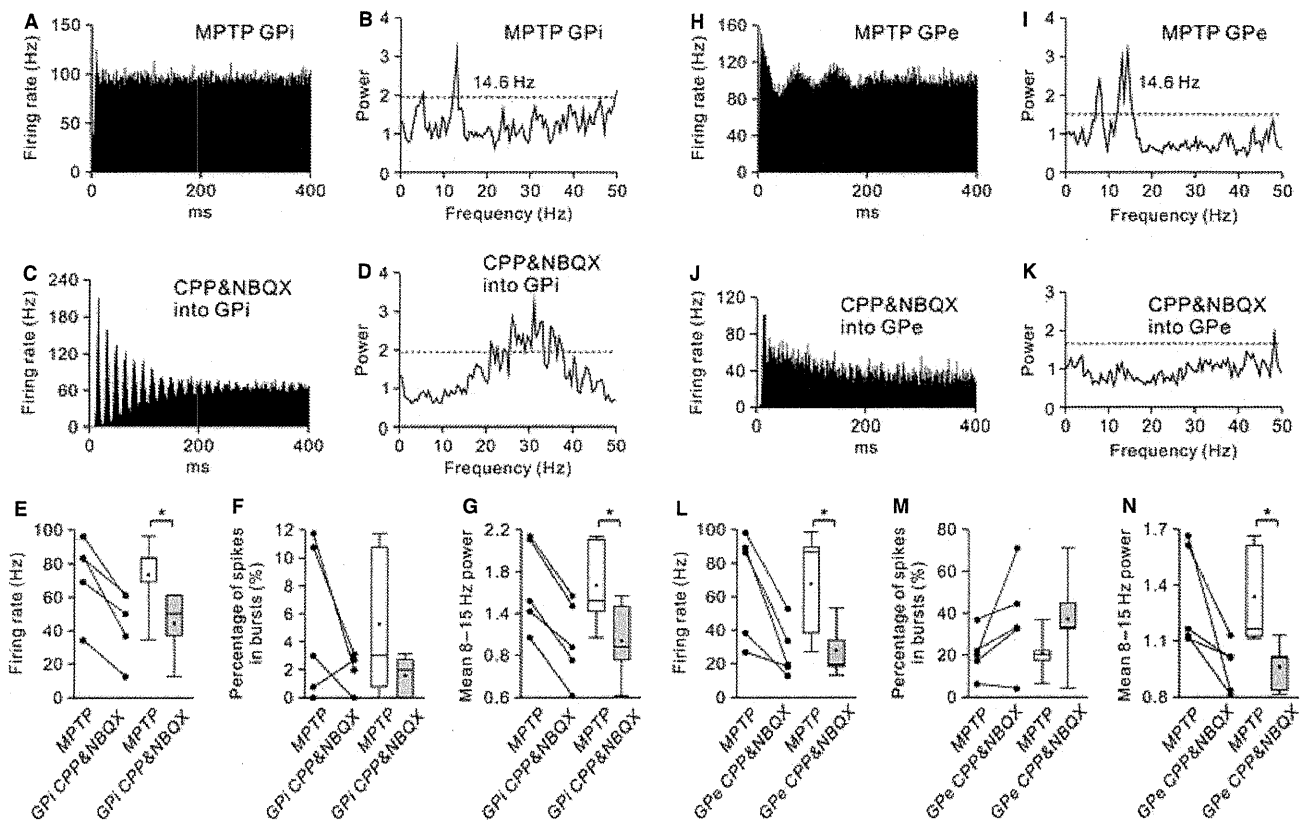


FIG. 9. Effects of intrapallidal blockade of ionotropic glutamatergic neurotransmission on dopamine-depleted GPI/GPe neurons. (A, B, H and I) A pallidal neuron (GPI, A and B; GPe, H and I) showed 3–8-Hz and 8–15-Hz oscillations in the parkinsonian state. (C, D, J and K) Microinjection of a mixture of CPP and NBQX in the vicinity of recorded GPI (C and D) and GPe (J and K) neurons decreased both the firing rates and oscillations. (E–G and L–N) Summaries of the effects of CPP and NBQX microinjections on the spontaneous firing rate (E and L), the burst strength (F and M) and the mean 8–15-Hz power spectrum of spike trains (G and N) in five GPI (E–G) and five GPe (L–N) neurons examined. Injections of CPP and NBQX significantly decreased the firing rate and the 8–15-Hz oscillatory power in the GPI and GPe. * $P < 0.05$.

Origins of abnormal 8–15-Hz oscillations in the GPI/GPe

The GPI and GPe receive glutamatergic inputs from the STN and GABAergic inputs from the striatum and/or GPe. To determine which inputs contribute to abnormal 8–15-Hz oscillations in the GPI, we first performed muscimol inactivation of the STN while simultaneously recording GPI neuronal activity (Fig. 1B). In all five cases, inactivation of the STN ameliorated parkinsonian motor signs, especially bradykinesia and rigidity, as previously reported (Bergman *et al.*, 1990; Wichmann *et al.*, 1994; Levy *et al.*, 2001b). The STN inactivation substantially decreased the 8–15-Hz oscillations (Fig. 8A–D and G; $P = 0.04$) and the firing rate (Fig. 8E; $P = 0.04$) in five GPI neurons, but no consistent changes were detected in the burst strength (Fig. 8F; $P = 0.89$). To obtain further evidence for subthalamic impacts on the oscillatory activity in the GPI/GPe, we also examined whether the intrapallidal blockade of ionotropic glutamate receptors could eliminate the GPI/GPe oscillations (Fig. 1C). Microinjection of a mixture of CPP and NBQX in the vicinity of recorded GPI/GPe neurons significantly decreased the average firing rate (Fig. 9A–D, H–K, E and L; $P = 0.04$ for both the GPI and GPe) and 8–15-Hz oscillations (Fig. 9G and N; $P = 0.04$ for both the GPI and GPe) in the GPI and GPe, whereas the burst strength was not changed uniformly in either structure (Fig. 9F and M; $P = 0.14$ for GPI; $P = 0.08$ for GPe).

We further tested whether GABAergic inputs from the striatum and/or GPe could affect the oscillatory activity of GPI/GPe neurons

(Fig. 1D). Microinjection of gabazine in the area surrounding recorded GPI/GPe neurons increased the firing rate of all of the neurons tested (Fig. 10A and C; $P = 0.02$ for GPI; $P = 0.04$ for GPe), and augmented the 8–15-Hz oscillations in the GPI (Fig. 10B; $P = 0.04$), but induced no significant changes in GPe oscillations (Fig. 10D; $P = 0.23$). The burst strength was not changed after the injections (GPI, $n = 7$, $P = 0.17$, Wilcoxon signed-rank test; GPe, $n = 5$, $P = 0.14$, Wilcoxon signed-rank test; data not shown). These results suggest that 8–15-Hz oscillations in the GPI/GPe originate from glutamatergic inputs mainly from the STN.

Origins of abnormal 8–15-Hz oscillations in the STN

The STN is known to receive glutamatergic inputs from the cerebral cortex and the thalamus, and GABAergic inputs from the GPe (Kitai & Deniau, 1981; Kita *et al.*, 1983; Bevan *et al.*, 1995). We first tested whether the elimination of ionotropic glutamatergic inputs could affect the generation of abnormal oscillatory activity in the STN (Fig. 1E). Local injections of a mixture of CPP and NBQX in the vicinity of recorded neurons suppressed the 8–15-Hz oscillations (Fig. 11A–D and G; $P = 0.03$), but increased their burst activities (Fig. 11F; $P = 0.03$), in six STN neurons tested. Such local injections did not induce consistent changes in the firing rate (Fig. 11E; $P = 0.84$).

We further examined whether the interruption of GPe-derived GABAergic inputs can suppress oscillations in the STN (Fig. 1F).

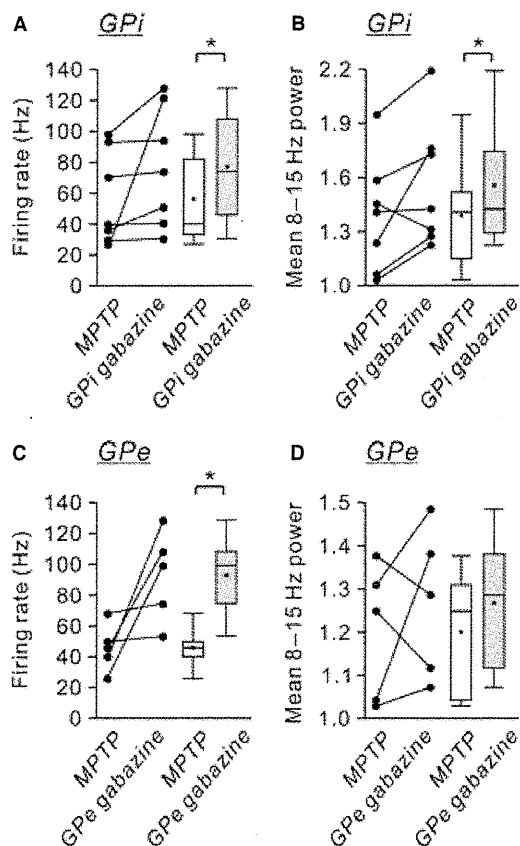


FIG. 10. Effects of intrapallidal blockade of ionotropic GABAergic neurotransmission on dopamine-depleted GPI/GPe neurons. Effects of intrapallidal gabazine microinjections on the spontaneous firing rate (A and C) and the mean 8–15-Hz power spectrum of spike trains (B and D) in seven GPI (A and B) and five GPe (C and D) neurons examined in the parkinsonian state. Injections of gabazine significantly increased the firing rates of GPI/GPe neurons, and increased the 8–15-Hz oscillatory power in the GPI. $*P < 0.05$.

Muscimol inactivation of the GPe attenuated the 8–15-Hz oscillations (Fig. 12A–D and G; $P = 0.03$) and the burst strength (Fig. 12F; $P = 0.03$), and increased the firing rate (Fig. 12E; $P = 0.03$), in six STN neurons tested. In contrast to muscimol inactivation of the STN, the GPe inactivation induced no clear behavioral changes. Taking these findings together, we conclude that the STN oscillatory rhythm is generated by both glutamatergic and GABAergic inputs to the STN.

Discussion

Our results show that loss of nigral dopamine neurons induced abnormal oscillations of GPI/GPe and STN neurons. The GPI/GPe and STN oscillations were reversed by systemic dopamine administration. Notably, direct manipulations of synaptic transmission within the BG of awake parkinsonian primates showed that STN oscillations induced oscillatory activity in the 8–15-Hz range in the GPI/GPe. We further demonstrated that the STN oscillations were strongly driven by (i) glutamatergic inputs, which are thought to arise mainly from the cortex, and (ii) GABAergic inputs from the GPe. These findings suggest that, in the dopamine-depleted state, glutamatergic inputs to the STN and reciprocal GPe–STN interconnections are both important for the generation and amplification of the oscillatory activity of STN neurons, which is subsequently transmitted to the GPI (Fig. 13).

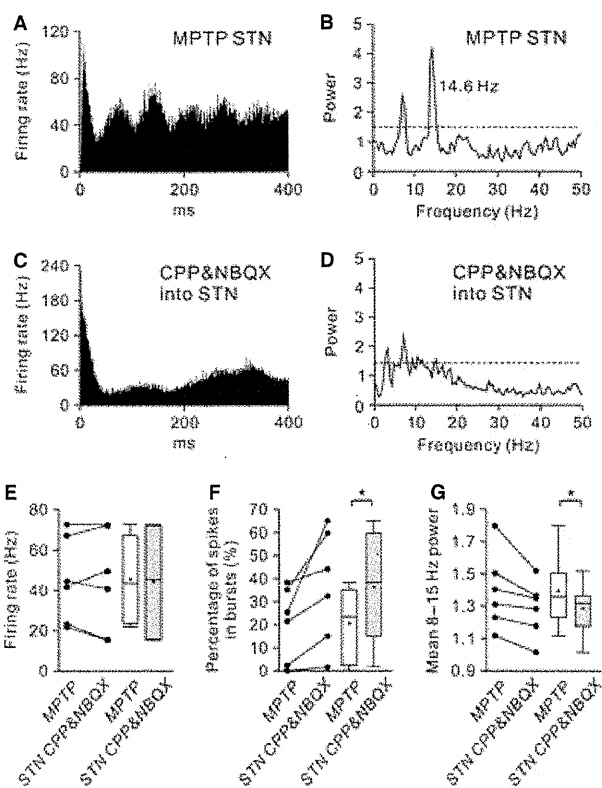


FIG. 11. Effects of intrasubthalamic blockade of ionotropic glutamatergic neurotransmission on dopamine-depleted STN neurons. (A and B) An STN neuron showed abnormal oscillatory bursts in the parkinsonian state. (C and D) Intrasubthalamic microinjection of a mixture of CPP and NBQX decreased 3–8-Hz and 8–15-Hz oscillations in the STN. On the other hand, the injection increased burst firing of the neuron. (E–G) Summaries of the effects of intrasubthalamic microinjections of CPP and NBQX on the spontaneous firing rate (E), the burst strength (F) and the mean 8–15-Hz power spectrum of spike trains (G) in six STN neurons examined. The microinjections of CPP and NBQX significantly decreased the 8–15-Hz oscillatory power, but increased the burst strength in the STN. $*P < 0.05$.

The classic model of PD pathophysiology suggests that degeneration of dopaminergic neurons leads to suppression of the striato-GPI ‘direct’ pathway and enhancement of the striato-GPe ‘indirect’ pathway; the increased GPI outputs attenuate thalamocortical neuron activity and induce parkinsonian motor signs (Albin *et al.*, 1989; DeLong, 1990). In this study, two MPTP-treated monkeys exhibited significant firing rate changes in STN neurons, but not in GPI neurons. Several reviews have emphasized that parkinsonism is directly related to BG oscillations (Boraud *et al.*, 2002; Brown, 2003; Gatev *et al.*, 2006; Rivlin-Etzion *et al.*, 2006a; Hammond *et al.*, 2007). The first goal of the present study was to test whether the abnormal BG oscillations depend on dopaminergic inputs. We confirmed that abnormal 8–15-Hz oscillations were increased in the GPI/GPe and STN of dopamine-depleted monkey brain, and were reversed after intravenous L-DOPA injections, with improvements in parkinsonian signs (Heimer *et al.*, 2006). Contrary to expectations, the firing rate of STN neurons increased following the L-DOPA injections. As in the striatum, L-DOPA might be converted to dopamine, which could be released from axon terminals of the remaining dopaminergic and serotonergic neurons in the STN (Lavoie & Parent, 1990; Francois *et al.*, 2000; Bezard *et al.*, 2001). Thus, L-DOPA could increase the firing rate of monkey

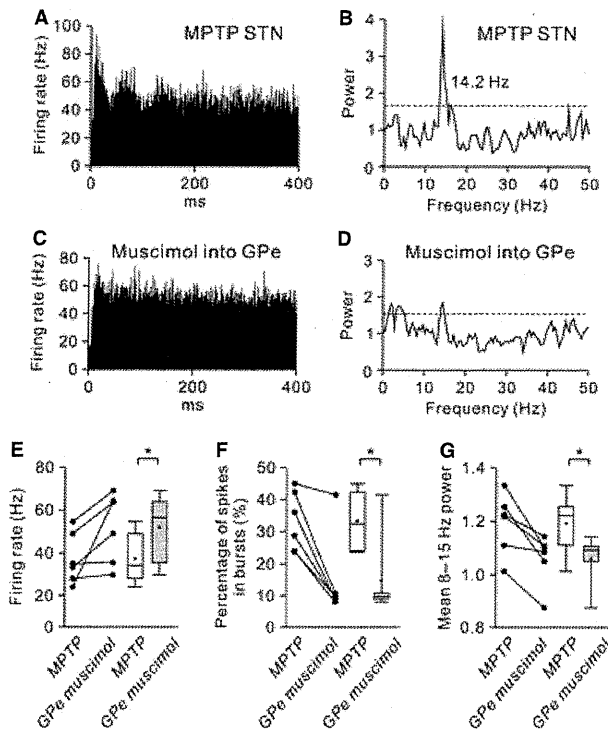


FIG. 12. Effects of GPe inactivation on dopamine-depleted STN neurons. (A and B) An STN neuron showed abnormal 8–15-Hz oscillations in the parkinsonian state. (C and D) Muscimol inactivation of the GPe decreased the 8–15-Hz oscillations in the STN, with an increase in the firing rate. (E–G) Summaries of the effects of muscimol inactivation of the GPe on the spontaneous firing rate (E), the burst strength (F) and the mean 8–15-Hz power spectrum of spike trains (G) in six STN neurons examined. Across the recorded population, the burst strength and the 8–15-Hz oscillations in the STN were decreased after GPe inactivation, whereas the GPe inactivation increased the firing rates of STN neurons. * $P < 0.05$.

STN neurons by eliciting the presynaptic suppression of GABAergic inputs via the direct activation of D2-like receptors (Shen & Johnson, 2000, 2005; Baufreton & Bevan, 2008).

We may predict that L-DOPA injections could reverse the decrease in the GPe firing rate after MPTP treatment. In contrast to previous reports that L-DOPA injections reversed the decrease in the rate of GPe neuron firing after MPTP treatment (Boraud *et al.*, 1998; Heimer *et al.*, 2006), we could not detect such a change uniformly. Increased STN activity may excite some GPe neurons, which may then inhibit other neighboring GPe neurons through GPe–GPe intranuclear axon collaterals (Kita & Kitai, 1994; Nambu & Llinás, 1997; Sato *et al.*, 2000). The data obtained from our L-DOPA studies suggest that normalization of neuronal oscillations in the GPi/GPe and STN may be more critical for L-DOPA actions in parkinsonian signs than changes in their spontaneous firing rates.

Our next aim was to determine the origin of 8–15-Hz oscillations of GPi/GPe neurons. The GPi/GPe receives glutamatergic inputs mainly from the STN and striatal GABAergic inputs (for review, see Smith *et al.*, 1998). The GPi/GPe also receives GABAergic inputs from the GPe through the GPe–GPi projection and the intranuclear collaterals (Hazrati *et al.*, 1990). However, no studies have demonstrated coherent activity between striatal projection neurons and GPi/GPe neurons. Here, we hypothesized that the GPi/GPe oscillations may be generated by glutamatergic inputs from the STN. Our findings revealed that STN inactivation simultaneously decreased the firing rate

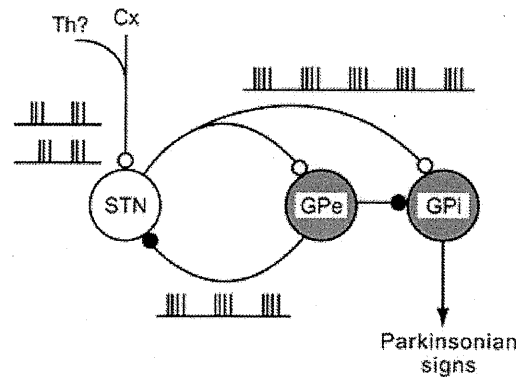


FIG. 13. Schematic diagram showing neural circuits involved in the generation of BG oscillations. In the dopamine-depleted state, a cooperative action of glutamatergic inputs from the cortex (Cx) [and perhaps also from the thalamus (Th)] and reciprocal GPe–STN interconnections can generate and amplify the oscillatory activity of STN neurons. The STN oscillations are finally transmitted to the GPi, thus contributing to the expression of parkinsonian motor signs. Open and filled circles represent glutamatergic and GABAergic synapses, respectively.

of GPi neurons, dampened their 8–15-Hz oscillations, and improved parkinsonian motor signs (see also Wichmann *et al.*, 1994). Moreover, microinjection of ionotropic glutamate receptor antagonists reduced the spontaneous firing rate and oscillatory activity in GPi/GPe neurons. In contrast, the 8–15-Hz oscillations were exaggerated or unchanged after microinjection of an ionotropic GABA receptor antagonist. These data suggest that the oscillatory events of GPi/GPe neurons are generated by glutamatergic inputs mainly from the STN, but not by GABAergic inputs from the striatum and GPe.

The final objective of this study was to elucidate the origin of 8–15-Hz oscillations in the STN. The glutamatergic afferents of the STN, which originate from the cortex and the thalamus, constitute one possibility (Kitai & Deniau, 1981; Bevan *et al.*, 1995). The present data showed that the STN oscillations were suppressed after the intrasubthalamic microinjection of ionotropic glutamate receptor antagonists. This suggests that the STN oscillations are partly formed by glutamatergic inputs to the STN. In accordance with the present result, estimates of coherence between the electrocorticogram and the STN LFPs/STN unit activity in the parkinsonian state have suggested that cortical glutamatergic inputs can drive STN oscillations in frequency bands below 30 Hz (Magill *et al.*, 2000, 2001; Sharott *et al.*, 2005; Mallet *et al.*, 2008b). The other possible glutamatergic sources of the primate STN are the intralaminar thalamic nuclei (Lanciego *et al.*, 2009). The parafascicular thalamic nucleus (PF) neurons in the rat PD model show some increased oscillatory activity (in the 0.5–2.5-Hz range) as compared with controls, but simultaneous recording of STN and PF neurons indicates that a majority of PF neurons fire after STN firing (Parr-Brownlie *et al.*, 2009). The contribution of thalamo-subthalamic glutamatergic afferents to STN oscillations needs to be further elucidated. Another candidate for the origin of STN oscillations comprises the GABAergic inputs from the GPe, which is interconnected with the STN (Baufreton *et al.*, 2005a). A recent *in vivo* rat study has indicated that dopamine depletion develops the 15–30-Hz oscillations between single GPe–STN neuron pairs (Mallet *et al.*, 2008a). We demonstrated that muscimol inactivation of the GPe attenuated the 8–15-Hz oscillatory activity of STN neurons and suppressed their burst firing properties. This result indicates that the GABAergic inputs from the GPe are likely to contribute to the production of the 8–15-Hz oscillatory bursts in the STN. The decrease in dopaminergic innervation of the GPe in MPTP-

treated monkeys (Schneider & Dacko, 1991) can augment the GPe–GPe GABAergic transmission (Watanabe *et al.*, 2009). The glutamatergic inputs with synchronized GABAergic inputs from the GPe may accelerate the rhythmic phase-locked activity in parkinsonian STN neurons, where dopaminergic innervation of the STN is lacking (Shen & Johnson, 2000, 2005; Baufreton *et al.*, 2005b; Baufreton & Bevan, 2008).

The present study focused on the 8–15-Hz oscillations in the BG of parkinsonian monkeys. LFPs recorded from the GPi/GPe and STN of parkinsonian rodents and PD patients exhibit dopamine-dependent synchronization in the higher 15–30-Hz range (Brown *et al.*, 2001; Cassidy *et al.*, 2002; Sharott *et al.*, 2005; Mallet *et al.*, 2008a,b). Single-unit recordings in the STN of PD patients, however, have demonstrated neuronal oscillations in the frequency range of 10–25 Hz (Levy *et al.*, 2000, 2002), similar to those in MPTP-treated monkeys. The discrepancy in peak frequencies among oscillation/synchronization might be attributable to the difference in the recording setup (Levy *et al.*, 2002), the extent to which loss of dopamine (including other catecholamines) progresses, depending on how parkinsonism is induced (Meredith *et al.*, 2008), and the species-specific intrinsic membrane properties of individual BG neurons and/or emergent properties of the cortico-BG circuit. The BG oscillations in the range below 30 Hz may constrain cortical processing via the BG–thalamocortical pathways (Engel & Fries, 2010). On the other hand, Leblois *et al.* (2007) have reported that oscillatory activity of BG neurons appears after the emergence of severe parkinsonian signs, and concluded that a causal relationship between BG oscillations and PD symptoms is unlikely. There is a possibility that the BG oscillations may merely reflect sensory inputs from the periphery in the states of akinesia/bradykinesia, rigidity, and tremor (Baker, 2007). Here, we simply emphasize that the BG oscillations disappeared when parkinsonian signs were alleviated. In fact, therapeutic approaches, such as dopaminergic medication and STN stimulation, and self-generated movements in human patients are known to decrease the cortico-BG synchronization (Brown *et al.*, 2001, 2004; Cassidy *et al.*, 2002; Levy *et al.*, 2002; Williams *et al.*, 2002; Silberstein *et al.*, 2005; Lafreniere-Roula *et al.*, 2010). In a similar manner, the suppression of the 8–15-Hz oscillations in the primate BG might be required to improve parkinsonian motor signs. We should also mention that BG dysfunction is associated with the abnormal ‘dynamic’ network properties in the dopamine-depleted BG, owing to the imbalance of neuronal processing between the ‘enhanced’ cortico-STN-GPi hyperdirect pathway and the ‘attenuated’ cortico-striato-GPi direct pathway. The BG oscillations generated in the hyperdirect pathway are suggested to serve to limit the ‘action selection’ properties processed in the direct pathway (Leblois *et al.*, 2006). In addition to the present data showing that STN inactivation suppressed the BG oscillations, our recent studies have revealed that cortically evoked inhibition in the GPi, which is induced via the direct pathway and associated with motor execution (Nambu *et al.*, 2000), is attenuated in the parkinsonian state and restored after STN inactivation (Nambu *et al.*, 2005; Kita & Kita, 2011). These findings suggest the importance of suppression of the ‘enhanced’ hyperdirect pathway in the reversal of parkinsonian motor signs. Our findings may shed light on the pathophysiology of PD and the exact mechanisms of many current therapies, and will help to develop improved treatments for PD patients.

Supporting Information

Additional supporting information may be found in the online version of this article:

Fig. S1. Three examples of burst detection using the ‘Poisson surprise’ algorithm.

Data S1. Behavioral criteria of the primate parkinsonian rating scale.

Please note: As a service to our authors and readers, this journal provides supporting information supplied by the authors. Such materials are peer-reviewed and may be re-organized for online delivery, but are not copy-edited or typeset by Wiley-Blackwell. Technical support issues arising from supporting information (other than missing files) should be addressed to the authors.

Acknowledgements

This study was supported by Grants-in-Aid for Scientific Research from the Ministry of Education, Culture, Sports, Science and Technology of Japan, the Japan Intractable Diseases Research Foundation and Hori Information Science Promotion Foundation to Y. Tachibana and A. Nambu, and NIH grants (NS-47085 and NS-57236) to H. Kita. We thank S. Yamamoto and I. Monosov for helpful comments and discussion, M. Meitzler for editing the manuscript, A. Ito, K. Miyamoto and M. Imanishi for technical assistance, and H. Toyoda for MRI scans.

Abbreviations

BG, basal ganglia; CPP, 3-(2-carboxypiperazin-4-yl)-propyl-1-phosphonic acid; GPe, external segment of the globus pallidus; GPi, internal segment of the globus pallidus; L-DOPA, L-3,4-dihydroxyphenylalanine; LFP, local field potential; MPTP, 1-methyl-4-phenyl-1,2,3,6-tetrahydropyridine; NBQX, 1,2,3,4-tetrahydro-6-nitro-2,3-dioxo-benzo[*q*]quinoxaline-7-sulfonamide; PD, Parkinson’s disease; PF, parafascicular thalamic nucleus; PSD, power spectral density; SD, standard deviation; STN, subthalamic nucleus; TH, tyrosine hydroxylase.

References

- Albin, R.L., Young, A.B. & Penney, J.B. (1989) The functional anatomy of basal ganglia disorders. *Trends Neurosci.*, **12**, 366–375.
- Baker, S.N. (2007) Oscillatory interactions between sensorimotor cortex and the periphery. *Curr. Opin. Neurobiol.*, **17**, 649–655.
- Baufreton, J. & Bevan, M.D. (2008) D2-like dopamine receptor-mediated modulation of activity-dependent plasticity at GABAergic synapses in the subthalamic nucleus. *J. Physiol.*, **586**, 2121–2142.
- Baufreton, J., Atherton, J.F., Surmeier, D.J. & Bevan, M.D. (2005a) Enhancement of excitatory synaptic integration by GABAergic inhibition in the subthalamic nucleus. *J. Neurosci.*, **25**, 8505–8517.
- Baufreton, J., Zhu, Z.T., Garret, M., Bioulac, B., Johnson, S.W. & Taupignon, A.I. (2005b) Dopamine receptors set the pattern of activity generated in subthalamic neurons. *FASEB J.*, **19**, 1771–1777.
- Bergman, H., Wichmann, T. & DeLong, M.R. (1990) Reversal of experimental parkinsonism by lesions of the subthalamic nucleus. *Science*, **249**, 1436–1438.
- Bergman, H., Wichmann, T., Karmon, B. & DeLong, M.R. (1994) The primate subthalamic nucleus. II. Neuronal activity in the MPTP model of parkinsonism. *J. Neurophysiol.*, **72**, 507–520.
- Bevan, M.D., Francis, C.M. & Bolam, J.P. (1995) The glutamate-enriched cortical and thalamic input to neurons in the subthalamic nucleus of the rat: convergence with GABA-positive terminals. *J. Comp. Neurol.*, **361**, 491–511.
- Bezard, E., Brotchie, J.M. & Gross, C.E. (2001) Pathophysiology of levodopa-induced dyskinesia: potential for new therapies. *Nat. Rev. Neurosci.*, **2**, 577–588.
- Boraud, T., Bezard, E., Guehl, D., Bioulac, B. & Gross, C. (1998) Effects of L-DOPA on neuronal activity of the globus pallidus externalis (GPe) and globus pallidus internalis (GPi) in the MPTP-treated monkey. *Brain Res.*, **787**, 157–160.
- Boraud, T., Bezard, E., Bioulac, B. & Gross, C.E. (2002) From single extracellular unit recording in experimental and human Parkinsonism to the development of a functional concept of the role played by the basal ganglia in motor control. *Prog. Neurobiol.*, **66**, 265–283.
- Brown, P. (2003) Oscillatory nature of human basal ganglia activity: relationship to the pathophysiology of Parkinson’s disease. *Mov. Disord.*, **18**, 357–363.

- Brown, P., Oliviero, A., Mazzone, P., Insola, A., Tonali, P. & Di Lazzaro, V. (2001) Dopamine dependency of oscillations between subthalamic nucleus and pallidum in Parkinson's disease. *J. Neurosci.*, **21**, 1033–1038.
- Brown, P., Mazzone, P., Oliviero, A., Altibrandi, M.G., Pilato, F., Tonali, P.A. & Di Lazzaro, V. (2004) Effects of stimulation of the subthalamic area on oscillatory pallidal activity in Parkinson's disease. *Exp. Neurol.*, **188**, 480–490.
- Cassidy, M., Mazzone, P., Oliviero, A., Insola, A., Tonali, P., Di Lazzaro, V. & Brown, P. (2002) Movement-related changes in synchronization in the human basal ganglia. *Brain*, **125**, 1235–1246.
- DeLong, M.R. (1990) Primate models of movement disorders of basal ganglia origin. *Trends Neurosci.*, **13**, 281–285.
- Engel, A.K. & Fries, P. (2010) Beta-band oscillations – signalling the status quo? *Curr. Opin. Neurobiol.*, **20**, 156–165.
- Filion, M. (1979) Effects of interruption of the nigrostriatal pathway and of dopaminergic agents on the spontaneous activity of globus pallidus neurons in the awake monkey. *Brain Res.*, **178**, 425–441.
- Francois, C., Savy, C., Jan, C., Tande, D., Hirsch, E.C. & Yelnik, J. (2000) Dopaminergic innervation of the subthalamic nucleus in the normal state, in MPTP-treated monkeys, and in Parkinson's disease patients. *J. Comp. Neurol.*, **425**, 121–129.
- Gatev, P., Darbin, O. & Wichmann, T. (2006) Oscillations in the basal ganglia under normal conditions and in movement disorders. *Mov. Disord.*, **21**, 1566–1577.
- Halliday, D.M., Rosenberg, J.R., Amjad, A.M., Breeze, P., Conway, B.A. & Farmer, S.F. (1995) A framework for the analysis of mixed time series/point process data-theory and application to the study of physiological tremor, single motor unit discharges and electromyograms. *Prog. Biophys. Mol. Biol.*, **64**, 237–278.
- Hammond, C., Bergman, H. & Brown, P. (2007) Pathological synchronization in Parkinson's disease: networks, models and treatments. *Trends Neurosci.*, **30**, 357–364.
- Hazrati, L.N., Parent, A., Mitchell, S. & Haber, S.N. (1990) Evidence for interconnections between the two segments of the globus pallidus in primates: a PHA-L anterograde tracing study. *Brain Res.*, **533**, 171–175.
- Heimer, G., Rivlin-Etzion, M., Bar-Gad, I., Goldberg, J.A., Haber, S.N. & Bergman, H. (2006) Dopamine replacement therapy does not restore the full spectrum of normal pallidal activity in the 1-methyl-4-phenyl-1,2,3,6-tetra-hydropyridine primate model of Parkinsonism. *J. Neurosci.*, **26**, 8101–8114.
- Kaneda, K., Imanishi, M., Nambu, A., Shigemoto, R. & Takada, M. (2003) Differential expression patterns of mGluR1 α in monkey nigral dopamine neurons. *Neuroreport*, **14**, 947–950.
- Kaneda, K., Tachibana, Y., Imanishi, M., Kita, H., Shigemoto, R., Nambu, A. & Takada, M. (2005) Down-regulation of metabotropic glutamate receptor 1 α in globus pallidus and substantia nigra of parkinsonian monkeys. *Eur. J. Neurosci.*, **22**, 3241–3254.
- Kita, H. & Kita, T. (2011) Cortical stimulation evokes abnormal responses in the dopamine-depleted rat basal ganglia. *J. Neurosci.*, **31**, 10311–10322.
- Kita, H. & Kitai, S.T. (1994) The morphology of globus pallidus projection neurons in the rat: an intracellular staining study. *Brain Res.*, **636**, 308–319.
- Kita, H., Chang, H.T. & Kitai, S.T. (1983) Pallidal inputs to subthalamus: intracellular analysis. *Brain Res.*, **264**, 255–265.
- Kitai, S.T. & Deniau, J.M. (1981) Cortical inputs to the subthalamus: intracellular analysis. *Brain Res.*, **214**, 411–415.
- Lafreniere-Roula, M., Darbin, O., Hutchison, W.D., Wichmann, T., Lozano, A.M. & Dostrovsky, J.O. (2010) Apomorphine reduces subthalamic neuronal entropy in parkinsonian patients. *Exp. Neurol.*, **225**, 455–458.
- Lanciego, J.L., Lopez, I.P., Rico, A.J., Aymeric, M.S., Perez-Manso, M., Conte, L., Combarro, C., Roda, E., Molina, C., Gonzalo, N., Castle, M., Tunon, T., Erro, E. & Barroso-Chinea, P. (2009) The search for a role of the caudal intralaminar nuclei in the pathophysiology of Parkinson's disease. *Brain Res. Bull.*, **78**, 55–59.
- Lavoie, B. & Parent, A. (1990) Immunohistochemical study of the serotonergic innervation of the basal ganglia in the squirrel monkey. *J. Comp. Neurol.*, **299**, 1–16.
- Leblois, A., Boraud, T., Meissner, W., Bergman, H. & Hansel, D. (2006) Competition between feedback loops underlies normal and pathological dynamics in the basal ganglia. *J. Neurosci.*, **26**, 3567–3583.
- Leblois, A., Meissner, W., Bioulac, B., Gross, C.E., Hansel, D. & Boraud, T. (2007) Late emergence of synchronized oscillatory activity in the pallidum during progressive Parkinsonism. *Eur. J. Neurosci.*, **26**, 1701–1713.
- Levy, R., Hutchison, W.D., Lozano, A.M. & Dostrovsky, J.O. (2000) High-frequency synchronization of neuronal activity in the subthalamic nucleus of parkinsonian patients with limb tremor. *J. Neurosci.*, **20**, 7766–7775.
- Levy, R., Dostrovsky, J.O., Lang, A.E., Sime, E., Hutchison, W.D. & Lozano, A.M. (2001a) Effects of apomorphine on subthalamic nucleus and globus pallidus internus neurons in patients with Parkinson's disease. *J. Neurophysiol.*, **86**, 249–260.
- Levy, R., Lang, A.E., Dostrovsky, J.O., Pahapill, P., Romas, J., Saint-Cyr, J., Hutchison, W.D. & Lozano, A.M. (2001b) Lidocaine and muscimol microinjections in subthalamic nucleus reverse Parkinsonian symptoms. *Brain*, **124**, 2105–2118.
- Levy, R., Ashby, P., Hutchison, W.D., Lang, A.E., Lozano, A.M. & Dostrovsky, J.O. (2002) Dependence of subthalamic nucleus oscillations on movement and dopamine in Parkinson's disease. *Brain*, **125**, 1196–1209.
- Magill, P.J., Bolam, J.P. & Bevan, M.D. (2000) Relationship of activity in the subthalamic nucleus-globus pallidus network to cortical electroencephalogram. *J. Neurosci.*, **20**, 820–833.
- Magill, P.J., Bolam, J.P. & Bevan, M.D. (2001) Dopamine regulates the impact of the cerebral cortex on the subthalamic nucleus-globus pallidus network. *Neuroscience*, **106**, 313–330.
- Mallet, N., Pogossyan, A., Marton, L.F., Bolam, J.P., Brown, P. & Magill, P.J. (2008a) Parkinsonian beta oscillations in the external globus pallidus and their relationship with subthalamic nucleus activity. *J. Neurosci.*, **28**, 14245–14258.
- Mallet, N., Pogossyan, A., Sharott, A., Csicsvari, J., Bolam, J.P., Brown, P. & Magill, P.J. (2008b) Disrupted dopamine transmission and the emergence of exaggerated beta oscillations in subthalamic nucleus and cerebral cortex. *J. Neurosci.*, **28**, 4795–4806.
- Meredith, G.E., Sonsalla, P.K. & Chesselet, M.F. (2008) Animal models of Parkinson's disease progression. *Acta Neuropathol.*, **115**, 385–398.
- Nambu, A. & Llinás, R. (1997) Morphology of globus pallidus neurons: its correlation with electrophysiology in guinea pig brain slices. *J. Comp. Neurol.*, **377**, 85–94.
- Nambu, A., Tokuno, H., Hamada, I., Kita, H., Imanishi, M., Akazawa, T., Ikeuchi, Y. & Hasegawa, N. (2000) Excitatory cortical inputs to pallidal neurons via the subthalamic nucleus in the monkey. *J. Neurophysiol.*, **84**, 289–300.
- Nambu, A., Tachibana, Y., Kaneda, K., Tokuno, H. & Takada, M. (2005) Dynamic model of basal ganglia functions and parkinson's disease. In Bolam, J.P., Ingham, C.A. & Magill, P.J. (Eds), *The Basal Ganglia VIII*. Springer, New York, pp. 307–312.
- Parr-Brownlie, L.C., Poloskey, S.L., Bergstrom, D.A. & Walters, J.R. (2009) Parafascicular thalamic nucleus activity in a rat model of Parkinson's disease. *Exp. Neurol.*, **217**, 269–281.
- Priori, A., Foffani, G., Pesenti, A., Tamma, F., Bianchi, A.M., Pellegrini, M., Locatelli, M., Moxon, K.A. & Villani, R.M. (2004) Rhythm-specific pharmacological modulation of subthalamic activity in Parkinson's disease. *Exp. Neurol.*, **189**, 369–379.
- Rivlin-Etzion, M., Marmor, O., Heimer, G., Raz, A., Nini, A. & Bergman, H. (2006a) Basal ganglia oscillations and pathophysiology of movement disorders. *Curr. Opin. Neurobiol.*, **16**, 629–637.
- Rivlin-Etzion, M., Ritov, Y., Heimer, G., Bergman, H. & Bar-Gad, I. (2006b) Local shuffling of spike trains boosts the accuracy of spike train spectral analysis. *J. Neurophysiol.*, **95**, 3245–3256.
- Sato, F., Lavallee, P., Levesque, M. & Parent, A. (2000) Single-axon tracing study of neurons of the external segment of the globus pallidus in primate. *J. Comp. Neurol.*, **417**, 17–31.
- Schneider, J.S. & Dacko, S. (1991) Relative sparing of the dopaminergic innervation of the globus pallidus in monkeys made hemi-parkinsonian by intracarotid MPTP infusion. *Brain Res.*, **556**, 292–296.
- Sharott, A., Magill, P.J., Harnack, D., Kupsch, A., Meissner, W. & Brown, P. (2005) Dopamine depletion increases the power and coherence of beta-oscillations in the cerebral cortex and subthalamic nucleus of the awake rat. *Eur. J. Neurosci.*, **21**, 1413–1422.
- Shen, K.Z. & Johnson, S.W. (2000) Presynaptic dopamine D2 and muscarinic M3 receptors inhibit excitatory and inhibitory transmission to rat subthalamic neurons *in vitro*. *J. Physiol.*, **525**(Pt 2), 331–341.
- Shen, K.Z. & Johnson, S.W. (2005) Dopamine depletion alters responses to glutamate and GABA in the rat subthalamic nucleus. *Neuroreport*, **16**, 171–174.
- Silberstein, P., Pogossyan, A., Kuhn, A.A., Hottot, G., Tisch, S., Kupsch, A., Dowsey-Limousin, P., Hariz, M.I. & Brown, P. (2005) Cortico-cortical coupling in Parkinson's disease and its modulation by therapy. *Brain*, **128**, 1277–1291.
- Smith, R.D., Zhang, Z., Kurlan, R., McDermott, M. & Gash, D.M. (1993) Developing a stable bilateral model of parkinsonism in rhesus monkeys. *Neuroscience*, **52**, 7–16.

- Smith, Y., Bevan, M.D., Shink, E. & Bolam, J.P. (1998) Microcircuitry of the direct and indirect pathways of the basal ganglia. *Neuroscience*, **86**, 353–387.
- Soares, J., Kliem, M.A., Betarbet, R., Greenamyre, J.T., Yamamoto, B. & Wichmann, T. (2004) Role of external pallidal segment in primate parkinsonism: comparison of the effects of 1-methyl-4-phenyl-1,2,3,6-tetrahydropyridine-induced parkinsonism and lesions of the external pallidal segment. *J. Neurosci.*, **24**, 6417–6426.
- Tachibana, Y., Kita, H., Chiken, S., Takada, M. & Nambu, A. (2008) Motor cortical control of internal pallidal activity through glutamatergic and GABAergic inputs in awake monkeys. *Eur. J. Neurosci.*, **27**, 238–253.
- Watanabe, K., Kita, T. & Kita, H. (2009) Presynaptic actions of D2-like receptors in the rat cortico-striato-globus pallidus disynaptic connection *in vitro*. *J. Neurophysiol.*, **101**, 665–671.
- Wichmann, T. & Soares, J. (2006) Neuronal firing before and after burst discharges in the monkey basal ganglia is predictably patterned in the normal state and altered in parkinsonism. *J. Neurophysiol.*, **95**, 2120–2133.
- Wichmann, T., Bergman, H. & DeLong, M.R. (1994) The primate subthalamic nucleus. III. Changes in motor behavior and neuronal activity in the internal pallidum induced by subthalamic inactivation in the MPTP model of parkinsonism. *J. Neurophysiol.*, **72**, 521–530.
- Williams, D., Tijssen, M., Van Bruggen, G., Bosch, A., Insola, A., Di Lazzaro, V., Mazzone, P., Oliviero, A., Quartarone, A., Speelman, H. & Brown, P. (2002) Dopamine-dependent changes in the functional connectivity between basal ganglia and cerebral cortex in humans. *Brain*, **125**, 1558–1569.
- Yamada, T., McGeer, P.L., Baimbridge, K.G. & McGeer, E.G. (1990) Relative sparing in Parkinson's disease of substantia nigra dopamine neurons containing calbindin-D28K. *Brain Res.*, **526**, 303–307.

Differential activity patterns of putaminal neurons with inputs from the primary motor cortex and supplementary motor area in behaving monkeys

Sayuki Takara,¹ Nobuhiko Hatanaka,¹ Masahiko Takada,^{2,3} and Atsushi Nambu¹

¹Division of System Neurophysiology, National Institute for Physiological Sciences and Department of Physiological Sciences, The Graduate University for Advanced Studies, Okazaki, Aichi, Japan; ²Department of System Neuroscience, Tokyo Metropolitan Institute for Neuroscience, Fuchu, Tokyo, Japan; and ³Systems Neuroscience Section, Primate Research Institute, Kyoto University, Inuyama, Aichi, Japan

Submitted 8 September 2010; accepted in final form 4 June 2011

Takara S, Hatanaka N, Takada M, Nambu A. Differential activity patterns of putaminal neurons with inputs from the primary motor cortex and supplementary motor area in behaving monkeys. *J Neurophysiol* 106: 1203–1217, 2011. First published June 8, 2011; doi:10.1152/jn.00768.2010.—Activity patterns of projection neurons in the putamen were investigated in behaving monkeys. Stimulating electrodes were implanted chronically into the proximal (MI_{proximal}) and distal (MI_{distal}) forelimb regions of the primary motor cortex (MI) and the forelimb region of the supplementary motor area (SMA). Cortical inputs to putaminal neurons were identified by excitatory orthodromic responses to stimulation of these motor cortices. Then, neuronal activity was recorded during the performance of a goal-directed reaching task with delay. Putaminal neurons with inputs from the MI and SMA showed different activity patterns, i.e., movement- and delay-related activity, during task performance. MI-recipient neurons increased activity in response to arm-reach movements, whereas SMA-recipient neurons increased activity during delay periods, as well as during movements. The activity pattern of MI + SMA-recipient neurons was of an intermediate type between those of MI- and SMA-recipient neurons. Approximately one-half of MI_{proximal}, SMA-, and MI + SMA-recipient neurons changed activities before the onset of movements, whereas a smaller number of MI_{distal}- and MI_{proximal} + _{distal}-recipient neurons did. Movement-related activity of MI-recipient neurons was modulated by target directions, whereas SMA- and MI + SMA-recipient neurons had a lower directional selectivity. MI-recipient neurons were located mainly in the ventrolateral part of the caudal aspect of the putamen, whereas SMA-recipient neurons were located in the dorsomedial part. MI + SMA-recipient neurons were found in between. The present results suggest that a subpopulation of putaminal neurons displays specific activity patterns depending on motor cortical inputs. Each subpopulation receives convergent or nonconvergent inputs from the MI and SMA, retains specific motor information, and sends it to the globus pallidus and the substantia nigra through the direct and indirect pathways of the basal ganglia.

basal ganglia; striatum; motor control; single-unit recording

THE PRIMATE STRIATUM, composed of the putamen, the caudate nucleus, and the ventral striatum, is a main input station of the basal ganglia and receives neural signals from wide areas of the cerebral cortex. Every single striatal projection neuron is estimated to receive diverse inputs from ~750 to 7,500 cortical neurons (Bennet and Wilson 2000), and thus cortical information is massively integrated within the striatum. The activity of striatal projection neurons is strongly modulated by local

interneurons that also receive cortical inputs (Tepper et al. 2008). The projection neurons finally send processed signals to the external and internal segments of the globus pallidus and the substantia nigra pars reticulata through the direct and indirect pathways of the basal ganglia. Therefore, to understand the functional roles of striatal projection neurons, it is essential to examine how information from various cortical areas is integrated and represented within the striatum.

Previous electrophysiological studies revealed that the patterns of neural activity differed among subregions of the putamen (Alexander and Crutcher 1990; Kimura et al. 1992; Lee and Assad 2003; Liles 1983; Schultz and Romo 1992). Neurons in the lateral part of the putamen increased activity simply in relation to movements, whereas those in the medial part showed complex activity changes, such as responses to visual stimuli. These different response patterns may reflect difference in cortical inputs. Actually, the forelimb region of the primary motor cortex (MI) projects mainly to the ventrolateral part of the caudal aspect of the putamen, and that of the supplementary motor area (SMA) projects predominantly to the dorsomedial part (Nambu et al. 2002; Takada et al. 1998a, b). The mediolateral central region of the putamen receives convergent inputs from both the MI and SMA. Thus the information about the forelimb movements from the MI and SMA is processed in a convergent or nonconvergent manner within the putamen. To investigate how such cortical inputs are processed and represented in the putaminal projection neurons, their activity during the performance of a goal-directed reaching task with delay was recorded after identification of cortical inputs by stimulation of the MI and SMA in the present study.

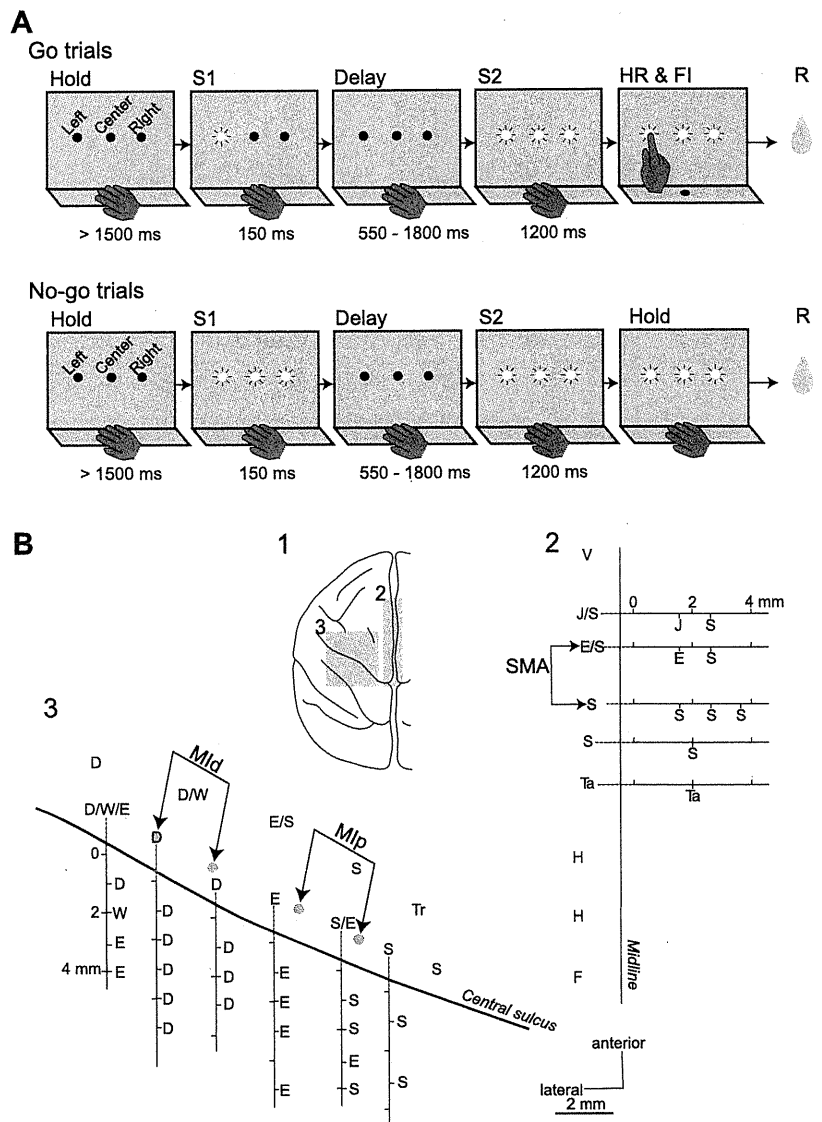
MATERIALS AND METHODS

Behavioral task. Two Japanese monkeys of either sex (*Macaca fuscata*; named S and A), weighing 5.2 and 8.0 kg, were used in this experiment. Both monkeys were right-handed. The experimental protocols were approved by the Institutional Animal Care and Use Committee of National Institutes of Natural Sciences, and all experiments were conducted according to the guidelines of the National Institutes of Health *Guide for the Care and Use of Laboratory Animals*.

Each animal was seated in a primate chair and trained to perform a goal-directed reaching task with delay (Fig. 1A). Three slots (Left, Center, and Right) were aligned horizontally in a panel that was placed at a distance of 30 cm in front of the animals. Three slots were separated from each other by 10 cm. Each slot was 18 mm in height, 6 mm in width, and 11 mm in depth. A two-color (red and green) light-emitting diode (LED) was installed in the bottom of each slot.

Address for reprint requests and other correspondence: A. Nambu, Division of System Neurophysiology, National Institute for Physiological Sciences, Myodaiji, Okazaki, Aichi 444-8585, Japan (e-mail: nambu@nips.ac.jp).

Fig. 1. A: goal-directed reaching task with delay. Three slots (Left, Center, and Right) were aligned horizontally in a panel that was placed in front of the animals. A 2-color (red and green) light-emitting diode (LED) was installed in the bottom of each slot. Each trial was initiated after the animal placed its hand at the resting position for at least 1,500 ms. In Go trials, 1 of the 3 LEDs (Left, Center, or Right) was lit with a red color for 150 ms as an instruction stimulus (S1). After a random delay period of 550–1,800 ms, all 3 LEDs were lit with a green color for 1,200 ms as a triggering stimulus (S2). Upon the presentation of the triggering stimulus, the monkey was required to reach out its forelimb and touch, using its index finger, the LED inside the slot that had been instructed previously by the S1. The timings of hand release (HR) from the resting position and of finger in (FI) the slot were detected by the infrared photoelectric sensors. If the monkey touched the correct LED within 1,200 ms, it was rewarded (R) with juice. In No-go trials, all 3 LEDs were lit simultaneously with a red color for 150 ms (S1). After a delay period of 550–1,800 ms, all 3 LEDs were lit with a green color for 1,200 ms (S2). If the monkey kept its hand at the resting position during these periods, it was rewarded with juice. B: cortical mapping (Monkey S) for implantation of stimulating electrodes. B1: top view of the monkey brain. Gray squares indicate mapped areas in 2 and 3. B2 and B3: mapping of the supplementary motor area (SMA) and primary motor cortex (MI), respectively. Each letter indicates the somatotopic body part: D, digit; E, elbow; F, foot; H, hip; J, jaw; S, shoulder; Ta, tail; Tr, trunk; V, visual response; W, wrist. Somatotopic arrangements in the mesial surface and the rostral bank of the central sulcus are also shown, along with depths from the cortical surface. Three pairs of bipolar-stimulating electrodes were implanted into the loci, indicated by small gray circles: the forearm region of the SMA and the proximal (Mip) and distal (Mid) forelimb regions of the MI.



Each trial was initiated after the animal placed its right hand at the resting position that was located below the panel for at least 1,500 ms. In Go trials (Fig. 1A), one of three LEDs was lit with a red color for 150 ms as an instruction stimulus. A random delay period of 550–1,800 ms followed the instruction stimulus. During the instruction stimulus and delay period, the monkey was required to keep its hand at the resting position. After a delay period, all three LEDs were lit with a green color for 1,200 ms as a triggering stimulus. Upon the presentation of a triggering stimulus, the monkey was required to reach out its right forelimb, using its index finger, and touch the LED inside the slot that had been directed previously by the instruction stimulus. The onset timings of the instruction stimulus and the triggering stimulus are denoted as S1 and S2, respectively. The timings of hand release (HR) from the resting position and finger in (FI) the slot were detected by infrared photoelectric sensors (Keyence, Osaka, Japan), installed in the resting position and slots. If the monkey touched the correct LED within 1,200 ms, it was rewarded with juice. The onset timing of reward delivery is denoted as R. If the monkey released its hand from the resting position during the instruction stimulus and delay period, touched the wrong LED, or touched the LED after 1,200 ms, it was not rewarded, and the trial with same task

conditions was repeated (repeat of the error conditions). In No-go trials (Fig. 1A), all three LEDs were lit simultaneously with a red color for 150 ms as an instruction stimulus. After a delay period of 550–1,800 ms, all three LEDs were lit with a green color for 1,200 ms as a triggering stimulus (S2). If the monkey kept its hand at the resting position during the entire delay and triggering-stimulus periods, it was rewarded with juice (R). If the monkey released its hand from the resting position during entire periods, it was not rewarded, and the No-go trial was repeated. Left, Center, and Right targets (appearance probability of each target, 29%) and No-go (13%) trials were presented randomly. Intertrial intervals (between the end of Reward and the beginning of the following trial) were 2,000–3,000 ms.

Surgery. After learning the behavioral task, the monkeys underwent surgical operations to fix their head painlessly in a stereotaxic frame attached to a primate chair (for details, see Nambu et al. 2000, 2002) under general anesthesia with sodium pentobarbital (25 mg/kg body wt, iv) after induction with ketamine hydrochloride (10 mg/kg im) and xylazine hydrochloride (1–2 mg/kg im).

After full recovery from the operation, the skull over the left MI and SMA was removed under light anesthesia with ketamine hydrochloride (10 mg/kg im) and xylazine hydrochloride (1–2 mg/kg im).

The forelimb regions of the MI and SMA were identified by electrophysiological methods (Fig. 1B; for details, see Nambu et al. 2000, 2002). According to this mapping, three pairs of bipolar-stimulating electrodes (made of 200 μm -diameter, enamel-coated, stainless-steel wires; intertip distance, 2 mm) were implanted chronically into the MI and SMA: one into the distal forelimb region of the MI ($\text{MI}_{\text{distal}}$), another into the proximal forelimb region of the MI ($\text{MI}_{\text{proximal}}$), and the other into the forelimb region of the SMA. Exposed areas were covered with transparent acrylic resin, except for the orofacial area of the MI (10–15 mm diameter), for access to the putamen. A rectangular plastic chamber covering the hole was fixed onto the skull with acrylic resin.

Single-unit recording of putaminal neurons. Recording neuronal activity of the left putamen was initiated after full recovery from the surgery and was performed 2 or 3 days/wk. During the experimental sessions, each monkey was seated in the monkey chair with head fixation. A glass-coated Elgiloy alloy microelectrode (0.5–1.5 $\text{M}\Omega$ at 1 kHz) was inserted obliquely (45° from vertical in the frontal plane) through the dura into the putamen to record neuronal activity using a hydraulic microdrive (Narishige Scientific Instrument Laboratory, Tokyo, Japan). The neuronal activity recorded from the microelectrode was amplified ($\times 10,000$), filtered (100–2,000 Hz), and displayed on an oscilloscope. The forelimb region of the putamen can be identified by 1) responses to sensory stimuli of the forelimb and 2) orthodromic excitation evoked by MI and SMA stimulation (Nambu et al. 2002). Activity of the putaminal neuron was isolated and converted into digital pulses using a time-amplitude window discriminator. The responses to cortical stimulation (300- μs duration single pulse, strength of < 0.6 mA, sometimes up to 0.7 mA, at 0.7 Hz) were observed by constructing peristimulus time histograms (PSTHs; bin width of 1 ms; summed for 100 stimulus trials) using a computer. During constructing PSTHs, the monkey sat quietly without performing any tasks. MI stimulation induced movements of corresponding body parts, but SMA stimulation did not. Only the neurons with apparent cortical inputs were sampled. To confirm the monosynaptic nature of orthodromic excitation, double-cortical stimulation with short intervals (20–50 ms) was applied in some neurons. Then, the neuronal activity during the performance of a goal-directed reaching task with delay was recorded. Timings of neuronal firings and task events (S1, S2, HR, FI, and R) were stored on a computer at a time resolution of 1 ms. These data, along with raw neuronal activity, were also stored on videotapes using a pulse-code modulation recorder (Cygnus Technology, Delaware Water Gap, PA). Finally, the responses of putaminal neurons to somatosensory stimuli, such as passive joint movements and muscle palpations and/or active forelimb movements, were examined.

During daily recording sessions, electromyograms (EMGs) were recorded five times for monkey S and six times for monkey A using surface electrodes from the following muscles: wrist extensor, wrist flexor, biceps brachii, triceps brachii, deltoid, trapezius, upper trunk, lower trunk, and quadriceps femoris. EMG signals were amplified, filtered (100–1,000 Hz), rectified, and stored on a computer.

Data analysis. On the basis of the firing frequency and patterns, putaminal neurons can be classified largely into two groups: phasically active neurons (PANs), which are silent at rest but phasically active during voluntary movements, and tonically active neurons (TANs), which exhibit tonic background discharges at ~ 2 –10 Hz and have longer spike duration than PANs (Alexander and DeLong 1985b; Aosaki et al. 1994; Kimura 1995). The majority of PANs are considered as medium, spiny γ -aminobutyric acid (GABA)ergic-projection neurons, whereas TANs are considered as large, spiny-cholinergic interneurons (Inokawa et al. 2010). In the present study, PANs, which met the following criteria, were sampled: 1) firing rate at rest not more than 5 Hz and 2) spike duration not more than 3 ms.

Responses to cortical stimulation were analyzed by PSTHs (summed for 100 stimulus trials). The mean value and SD of the firing rate during 100 ms, preceding the onset of stimulation, were calcu-

lated from PSTHs and were considered to be the value for base discharge (spontaneous firing rate). Responses to the cortical stimuli were judged to be significant if the firing rate during at least three consecutive bins (3 ms) reached the significant level of base discharge + 2 SD ($P = 0.0228$). The latency of the response was defined as the time at which the firing rate first exceeded this level. The responses whose latencies were < 21 ms were investigated in this study, as they were mediated by the direct corticostriatal projections based on our previous study (Nambu et al. 2002; see also DISCUSSION).

Neuronal activity during task performance was aligned with the task events (S1, S2, HR, FI, and R) separately, according to the S1 conditions (Left, Center, and Right targets and No-go trials) and shown in raster display. Then, spike-density functions ($\sigma = 13$ ms) were calculated. For detecting delay-related activity, the mean value and SD of the firing rate during 1,000 ms, preceding the S1, were calculated and were considered to be the value for base discharge. Activity changes during the delay periods were judged to be significant if the firing rate reached continuously the significant level of mean discharge + 2 SD ($P = 0.0228$) during at least 3 ms before the S2 (see Anderson and Horak 1985). For detecting movement-related activity, the mean value and SD of the firing rate during 500 ms, preceding the S2, were calculated. Activity changes during the arm-reach movements were judged to be significant if the firing rate reached continuously the significant level of mean discharge + 2 SD ($P = 0.0228$) during at least 3 ms in a 1,200-ms period centered at the HR. The periods of arm-reach movements include the timing of the FI. The latency of the neural response in reference to specific events, such as S1 and HR, was defined as the time at which the firing rate first exceeded this level (mean discharge + 2 SD for 3 ms), aligned with corresponding events. Amplitude (A) of responses related to each event was defined as the averaged number of spikes during the following periods: delay-related activity, a 500-ms period before the S2; HR-related activity, a 1,000-ms period centered at the HR; FI-related activity, a 1,000-ms period centered at the FI. Responses of delay-, HR-, and FI-related activity were modulated by target directions. Directional selectivity of each neuron in each event was defined as: directional selectivity = $1 - (A_{\text{med}} + A_{\text{min}})/(A_{\text{max}} \times 2)$, where A_{max} , A_{med} , and A_{min} are the maximum, medium, and minimum amplitudes among three targets, respectively ($0 \leq$ directional selectivity ≤ 1 ; directional selectivity = 0 means the same amplitude among three targets). In each neuron, spike-density histograms, showing the largest changes among three targets, were selected. Population activity was calculated by averaging spike-density histograms. The latency of the neuron was defined as the latency of the neural response with the largest changes among three targets.

EMG activity was also analyzed using similar methods. EMG activity during task performance was averaged with the task events separately, according to the S1 conditions. The mean value and SD of the activity during 1,000 ms, preceding the S1, were calculated and were considered to be the values for base activity. EMG activity changes were judged to be significant if the activity reached the significant level of base activity + 2 SD during at least 3 ms. The latency of the EMG activity was defined as the time at which the activity first exceeded this level.

Histology. At the end of the final experiment, several recording sites were marked by passing cathodal direct current (20 μA for 30 s) through the electrode. The monkeys were then anesthetized deeply with sodium pentobarbital (50 mg/kg iv) and perfused transcardially with 2 l of PBS, pH 7.3, followed by 5 l of 8% formalin in 0.1 M phosphate buffer (PB), pH 7.3, and 3 l of 0.1 M PB containing 10% sucrose. The brains were removed, kept in 0.1 M PB containing 30% sucrose at 4°C, and then cut serially into 50 μm -thick frontal sections on a freezing microtome. The sections were mounted onto gelatin-coated glass slides and stained with cresyl violet. The recording sites were reconstructed according to the lesions made by current injection and the traces of electrode tracks. The positions of cortical stimulation electrodes were also confirmed histologically.

RESULTS

EMG activity. Figure 2 shows a typical example of EMG activity during task performance. EMG activity was aligned with HR (Go trials, at *time 0*) or S2 (No-go trials) and averaged separately, according to the S1 conditions. In Go trials, no significant activity changes were observed during the delay period. Large activity increase in forelimb muscles, such as the wrist extensor, wrist flexor, and biceps brachii muscles began preceding the HR. Among them, the biceps brachii muscle displayed the earliest EMG changes, preceding the HR by 170 ms. This activity before the HR may contribute to HR from the resting position. The wrist extensor, biceps brachii, and deltoid muscles showed different activities among Left, Center, and Right target trials, and this may determine the direction of reaching. The wrist flexor and extensor muscles showed large EMG activity 200–600 ms after the HR and may contribute to hand shaping at the final stage of reaching. The upper-trunk muscles were also active during movements, whereas no obvious activity was observed in the lower trunk or hindlimbs. In No-go trials, no significant changes of EMG activity were detected.

Spontaneous firing rates. In the present study, a total of 821 putamen neurons, which were classified as PANs, was sampled in two monkeys. Among them, 447 neurons displayed significant excitatory responses to cortical stimulation based on offline analysis and were studied further. The second stimulation of the double-cortical stimulation evoked comparable excitatory responses with those evoked by the first stimulation (data not shown), suggesting that the excitatory responses were mediated by direct corticostriatal projections. According to the cortical inputs, putamen neurons were classified into three groups: MI-, SMA-, and MI + SMA-recipient neurons (Nambu et al. 2002). MI-recipient neurons were further classified into MI_{proximal}-, MI_{distal}-, and MI_{proximal + distal}-recipient neurons. MI + SMA-recipient neurons were also classified into MI_{proximal} + SMA-, MI_{distal} + SMA-, and MI_{proximal + distal} + SMA-recipient neurons. The number of neurons belonging to each group and their spontaneous firing rates are shown in Table 1. A considerable number of neurons received convergent inputs from multiple cortical areas. The spontaneous firing rate of MI-recipient neurons [1.41 ± 1.82 (SD) Hz] was significantly lower than those of SMA (2.50 ± 2.67

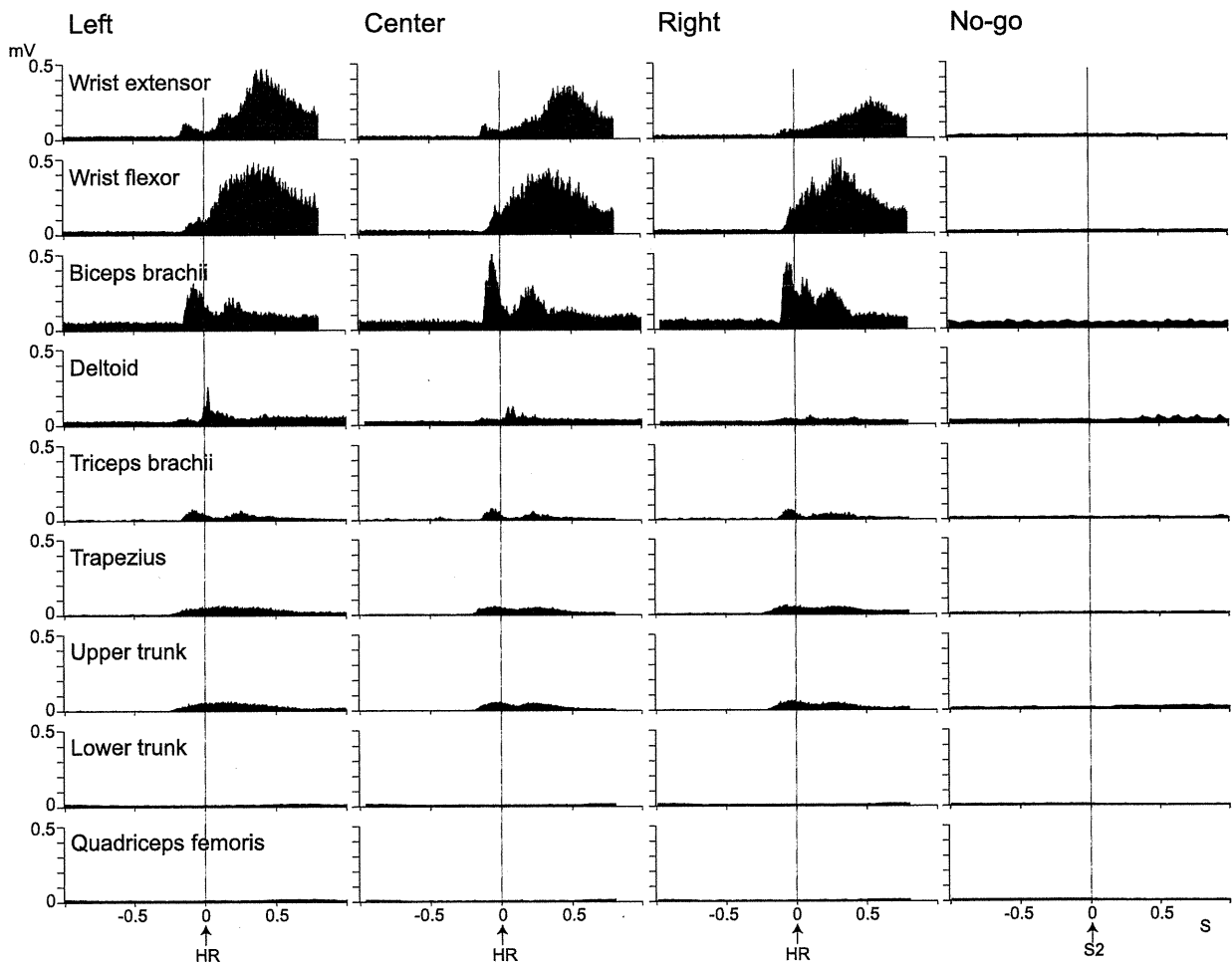


Fig. 2. Electromyogram (EMG) activity during the performance of a goal-directed reaching task with delay. EMG activity was rectified, aligned at the HR (Go trials, at *time 0*) or S2 (No-go trials), and averaged 100 times separately, according to the S1 conditions (Left, Center, and Right targets and No-go trials). In Go trials, EMG activity was observed in the forelimb and upper-trunk muscles but not in the lower-trunk and hindlimb muscles. No EMG activity was observed in No-go trials.

Table 1. Classification of putaminal neurons and their spontaneous firing rates

Cortical inputs	Number of neurons			Spontaneous firing rate (mean \pm SD, Hz)
	Monkey S	Monkey A	Total	
MI			246 (55)	1.41 \pm 1.82*,†
MI _{proximal}	40	76	116 (26)	1.34 \pm 1.70
MI _{distal}	26	40	66 (15)	1.40 \pm 1.99
MI _{proximal} + distal	21	43	64 (14)	1.77 \pm 1.84
SMA	50	60	110 (25)	2.50 \pm 2.67*
MI + SMA			91 (20)	2.48 \pm 2.20†
MI _{proximal} + SMA	20	26	46 (10)	2.18 \pm 1.86
MI _{distal} + SMA	8	20	28 (6)	2.18 \pm 2.51
MI _{proximal} + distal + SMA	5	12	17 (4)	3.66 \pm 2.24
Total	170	277	447 (100%)	1.90 \pm 2.17

Numbers of putaminal neurons in two monkeys and their spontaneous firing rates are shown according to cortical inputs. Figures in parentheses indicate the percentage to the total number of neurons. Spontaneous firing rates were calculated from peristimulus time histograms during 100 ms preceding the onset of cortical stimulation without any behavioral tasks (see MATERIALS AND METHODS). MI_{distal} and MI_{proximal}, distal and proximal forelimb regions of the primary motor cortex, respectively; SMA, forelimb region of the supplementary motor area. *, †Significantly different from each other (Bonferroni/Dunn post hoc tests; $P < 0.05$).

Hz)- and MI + SMA (2.48 ± 2.20 Hz)-recipient neurons ($P < 0.05$; Bonferroni/Dunn post hoc tests).

The latencies of excitations in putaminal neurons evoked by each cortical stimulation are compared in Fig. 3. The latency of MI_{proximal}-induced excitation (10.9 ± 2.5 ms; Fig. 3A) and that of MI_{distal}-induced excitation (11.5 ± 2.6 ms; Fig. 3B) was significantly shorter than that of SMA-induced excitation (14.1 ± 2.8 ms; Fig. 3C; Bonferroni/Dunn post hoc tests; $P < 0.05$). The latencies of the excitation evoked by stimulation

in the same cortical area were comparable between neurons with converging inputs and neurons with a single cortical input (Fig. 3).

Activity during task performance. Activity of putaminal neurons with different cortical inputs is exemplified in Figs. 4–6. Figure 4A shows a typical example of MI_{proximal}-recipient putaminal neurons. This neuron received cortical input exclusively from the MI_{proximal}. MI_{proximal} stimulation evoked excitatory responses at a latency of 11 ms (Fig. 4A1), whereas stimulation of other cortical areas did not. Neuronal activity during task performance was aligned with the S1 and HR (Go trials) or the S1 and S2 (No-go trials) separately, according to the S1 conditions, and averaged (Fig. 4A2). This neuron exhibited no activity during the delay period and increased activity in relation to arm-reach movements, preceding the HR by 125 ms. The amplitude of movement-related activity was larger in the Right target trials than in the Center and Left target trials. Directional selectivity of the HR-related activity was 0.60. No activity was observed in No-go trials. Somatosensory examination revealed that this neuron was activated by lateral rotation of the shoulder. These observations suggest that this neuron increased activity in relation to the proximal forelimb movement, such as HR from the resting position.

Figure 4B shows a typical example of MI_{distal}-recipient putaminal neurons. This neuron received cortical input exclusively from the MI_{distal}. MI_{distal} stimulation evoked excitatory responses at a latency of 15 ms (Fig. 4B1), whereas stimulation of other cortical areas did not. This neuron exhibited no activity during the delay period (Fig. 4B2). This neuron showed a mild activity increase after the HR in the Right target trials and a large activity increase around the FI in all three targets conditions. The timing-of-activity increase correlated with the FI, not with the S2, HR, or R. No activity was observed in No-go trials. Directional selectivity of the FI-related activity was 0.21. This neuron was activated by abduction of the wrist. These observations suggest that this neuron increased activity in relation to the distal forelimb movement, such as shaping its hand for touching the target slot.

Figure 5, A and B, shows two examples of SMA-recipient putaminal neurons. These neurons received cortical input exclusively from the SMA. The neuron in Fig. 5A responded

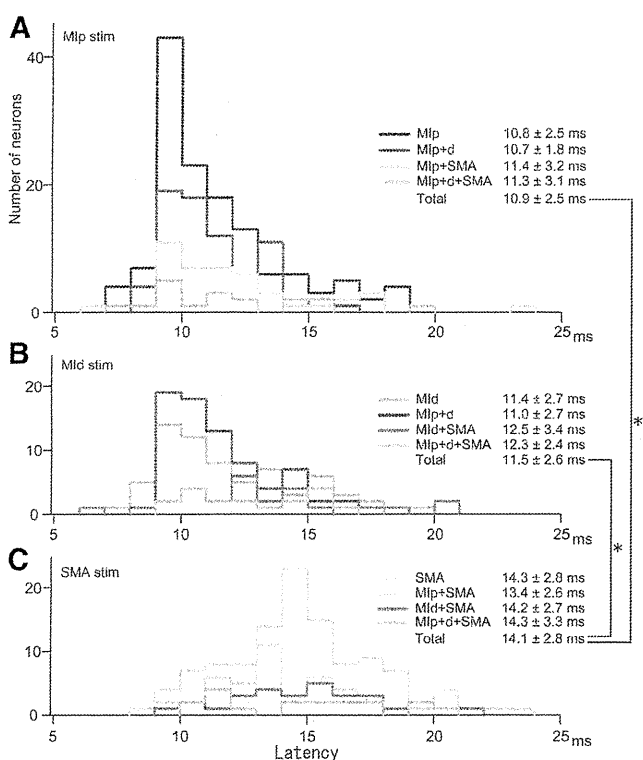
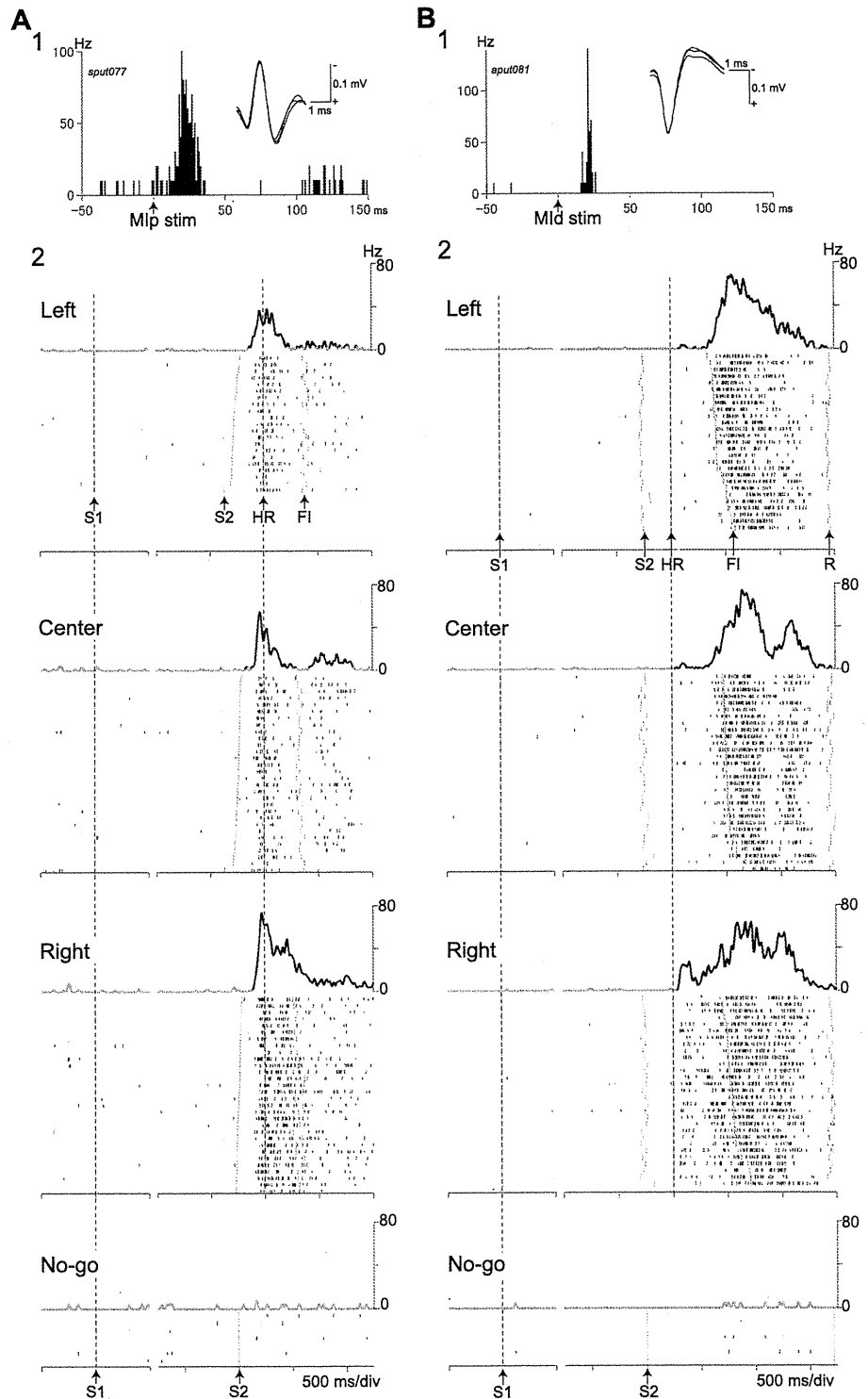


Fig. 3. Distribution of the latencies of cortically evoked excitatory responses in putaminal neurons. Ordinates indicate the number of neurons. A: latencies of MI- and MI + SMA-recipient neurons to MI_{proximal} stimulation. B: latencies of MI- and MI + SMA-recipient neurons to MI_{distal} stimulation. C: latencies of SMA- and MI + SMA-recipient neurons to SMA stimulation. *Significantly different from each other (Bonferroni/Dunn post hoc tests; $P < 0.05$).

Fig. 4. *A*: typical example of $MI_{proximal}$ -recipient putamen neurons. *A1*: peristimulus time histograms (PSTHs; bin width of 1 ms; 100 stimulus trials) showing responses to $MI_{proximal}$ stimulation (duration 300 μ s, single pulse, 0.4 mA). Voltage traces of action potentials are shown as an inset. *A2*: raster display showing the neuronal firing (short, black vertical lines) during the performance of a goal-directed reaching task with delay. Neuronal activity was aligned separately according to the S1 conditions (Left, Center, and Right targets and No-go trials, from top to bottom) with the S1 (left), and HR (right; in Go trials) or S2 (right; in No-go trials). Short, gray vertical lines indicate the timing of the S2 and FI. Each plot of Go trials was sorted according to the reaction time (S2-HR). Continuous, gray traces indicate spike-density functions ($\sigma = 13$ ms) for the associated rasters. For the spike-density functions in this and the following figures, the mean value and SD of the firing rate during 1,000 ms, preceding the S1, were calculated. The spike-density functions with significant changes, which continuously reach the significant level of mean discharge + 2 SD during at least 3 ms, are indicated by black traces. Abscissa, ticked every 500 ms. *B*: typical example of MI_{distal} -recipient putamen neurons. *B1*: PSTHs showing responses to MI_{distal} stimulation (0.4 mA). *B2*: raster display showing the neuronal firing during task performance. Each plot of Go trials was sorted according to the movement time (HR-FI). The timing of the R is also indicated by short, gray vertical lines.



to SMA stimulation at a latency of 12 ms (Fig. 5A1), whereas stimulation of other cortical areas did not. This neuron showed delay-related activity, i.e., a gradual firing-rate increase beginning after the S1 and lasting before S2 (Fig. 5A2). Delay-related activity was observed in all three target conditions, and directional selectivity of delay-related

activity was 0.21. The activity increased additionally and reached its peak after the HR, suggesting that this neuron also showed movement-related activity. Although the activity increase was also observed in No-go trials, its amplitude was smaller than that in Go trials. This neuron was activated during active shoulder movements. Figure 5B shows another